

HEAT-FLOW MEASUREMENTS AT SHOT POINTS ALONG THE 1978
SAUDI ARABIAN SEISMIC DEEP-REFRACTION LINE,
PART 2: DISCUSSION AND INTERPRETATION

by

M. E. Gettings

U.S. Geological Survey
Open-File Report 82-794

This report is preliminary and has not been reviewed for conformity with U.S. Geological Survey editorial standards and stratigraphic nomenclature. Any use of trade names is for descriptive purposes only and does not imply endorsement by the USGS.

Report prepared for
Ministry of Petroleum and Mineral Resources
Deputy Ministry for Mineral Resources
Jiddah, Kingdom of Saudi Arabia
1402 AH 1982 AD

CONTENTS

	<u>Page</u>
ABSTRACT.....	1
INTRODUCTION.....	2
A MODEL FOR THE LITHOSPHERE OF THE SOUTHERN RED SEA AND ADJOINING ARABIAN PENINSULA.....	7
GEOTERM ESTIMATES FOR THE ARABIAN SHIELD.....	14
SOME THERMAL MODELS FOR THE OCEANIC LITHOSPHERE.....	18
Estimates of parameter values.....	18
Thermal conductivity and diffusivity.....	18
Spreading velocities and strain rates.....	19
Radiogenic heat-source distributions.....	20
Static models for the shelf area.....	21
Dynamic models for the oceanic crust.....	24
Edge effects at shot point 5.....	26
SUMMARY.....	28
REFERENCES.....	29
APPENDIX 1. Static cooling of an infinite sheet.....	34
2. Temperature and heat flow of a homogeneous quarter-space.....	38

ILLUSTRATIONS

Figure 1. Generalized geologic map showing locations of the shot points and of other heat-flow data points.....	3
2. Plot of heat-flow values as a function of distance from the Red Sea deep-water axis.....	5
3. Plot of heat flow as a function of heat generation for three plutonic rocks of the Arabian Shield.....	6
4a. Generalized topographic profile for the southern Arabia-Red Sea-East Africa area.....	8
b. Average topographic and generalized geochronological profile for southern Saudi Arabia as a function of distance from the Red Sea deep-water axis.....	8
5. Schematic crustal cross section for the southwestern Saudi Arabia-southern Red Sea area.....	13
6. Graph showing geotherm estimates for the Arabian Shield at shot points 2, 3, and 4.....	16
7. Graphs showing geotherm estimates for the shelf and coastal-plain areas, static and dynamic models.....	22
8. Plots showing heat-flow and temperature-depth curves for static cooling of a horizontal sheet.....	23

	<u>Page</u>
9. Plots of surface heat flow for boundary heating of quarter-space.....	27
10. Geometric relationships and parameters for the static cooling of a horizontal sheet.....	35
11. Geometric relationships and parameters for a homogeneous quarter-space.....	35

TABLE

Table 1.	Heat-flow estimates from drill holes at shot points 1, 2, 3, 4, and 5, along the seismic refraction line, Kingdom of Saudi Arabia.....	4
----------	--	---

HEAT-FLOW MEASUREMENTS AT SHOT POINTS ALONG THE 1978
SAUDI ARABIAN SEISMIC DEEP-REFRACTION LINE,
PART 2: DISCUSSION AND INTERPRETATION

by

M. E. Gettings

ABSTRACT

The heat-flow profile across the Arabian Shield from Ar Riyad to Ad Darb and across the Red Sea is examined for compatibility with the lithospheric structure of the area as deduced from geologic and other geophysical data. Broad continental uplift associated with Red Sea rifting is symmetric about the Red Sea axis, and geologic and geochronologic evidence indicate that uplift has occurred mainly in the interval 25-13 Ma (mega-annum) ago. Thermal-profile changes in the upper mantle resulting from an influx of hot material associated with rifting yield the correct order of magnitude of uplift, and this mechanism is suggested as the explanation for the regional doming. A lithospheric section, constructed from seismic refraction, gravity, and regional geologic data, provides the framework for construction of thermal models.

Thermal gradient measurements were made in drill holes at five shot points. Geotherms for the Shield, which assume a radiogenic heat-source distribution that decreases exponentially with depth, yield temperatures of about 450°C at a depth of 40 km (base of the crust) for shot points 2 (Sabhah) and 3. The geotherm for shot point 4 (near Bishah) yields a distinctly higher temperature (about 580°C) for the same depth.

Static models used to model the heat flow in the oceanic crust of the Red Sea shelf and coastal plain either yield too small a heat flow to match the observed heat flow or give lithosphere thicknesses that are so thin as to be improbable. Dynamic (solid-state accretion) models, which account for mantle flow at the base of the lithosphere, adequately match the observed heat-flow values. In the deep-water trough of the Red Sea, which is presently undergoing active sea-floor spreading, classical models of heat flow for a moving slab with accretion at the spreading center are adequate to explain the average heat-flow level.

At shot point 5 (Ad Darb), the anomalous heat flow of 2 HFU (heat-flow units) can be explained in terms of a Shield component (0.8-1.0 HFU) and a component related to heating by the abutting oceanic crust a few kilometers away for periods exceeding 10 Ma. Analytical results are included for: 1) the cooling of a static sheet with an initial temperature distribution characteristic of a moving slab in a sea-floor spreading environment, and 2) the heating of a homogeneous quarter-space at its vertical boundary.

INTRODUCTION

Five heat-flow measurements at intervals roughly 200 km long across the Arabian Shield from Ar Riyad to Ad Darb were completed in January and February, 1978. Temperature-logging measurements were made in most of the pattern boreholes, approximately 60 m deep, at each of five on-land shot points (SP) of the 1978 seismic deep-refraction line. Location of the shot points and a generalized geologic map of the area are shown in figure 1. The estimation of heat-flow and heat-generation values and their uncertainties is described in a companion report (Gettings and Showail, 1982); the resulting data are summarized in table 1 and figures 2 and 3. In figure 2, the heat-flow profile has been extended to include a heat-flow measurement from a deep borehole on the coastal plain (Mansiyah I, Girdler, 1970) and marine heat-flow measurements (Girdler and Evans, 1977) in both the shallow-and deep-water areas of the Red Sea in a swath 200 km wide that trends 236° across the Red Sea. The center line of the swath was chosen so as to pass through shot point 6 (fig. 1).

The dominant characteristic of the resulting profile (fig. 2) is a three-level pattern: 1) about 4 HFU (heat-flow unit, $1 \text{ HFU} = 0.041868 \text{ Wm}^{-2}$) over the presently active spreading center (axial trough); 2) about 3 HFU over the Red Sea shelf areas corresponding to the first stage of spreading (Girdler and Styles, 1974); and 3) about 1 HFU over the Precambrian Arabian Shield. Shot point 5 is on the Shield but has a higher heat flow (2 HFU) than other points on the Shield; this is presumably due to heating by Tertiary oceanic crust, which is only a few kilometers away. The limited data available (three points, fig. 3) suggest that no linear relation exists between heat flow and heat generation in the Arabian Shield, at least within approximately 200 km of the edge of the oceanic crust.

This report presents the results of an investigation of the compatibility of the heat-flow profile with some models of the structure of the lithosphere and asthenosphere in the southern Arabian Shield and southern Red Sea. Detailed descriptions of these models and the geologic and geophysical evidence supporting them are presented elsewhere (Blank and Gettings, unpub. data; Gettings and Blank, unpub. data). I begin here with a brief summary of the relevant geophysical and geological data in this area and develop a general lithospheric model, which I generalize for my purposes into three provinces. Next I estimate the relevant physical properties and construct by conventional methods continental geotherm estimates for heat-flow observations on the Shield. I then investigate several possible models of the thermal regime in the oceanic lithosphere of Red Sea and attempt to set bounds on possible geotherms consistent with the geophysical data. Finally, I discuss some implications of the high heat flow at shot point 5 and suggest that a detailed heat-flow profile onto the Shield perpendicular to the boundary between the oceanic and continental crust might yield fruitful results.

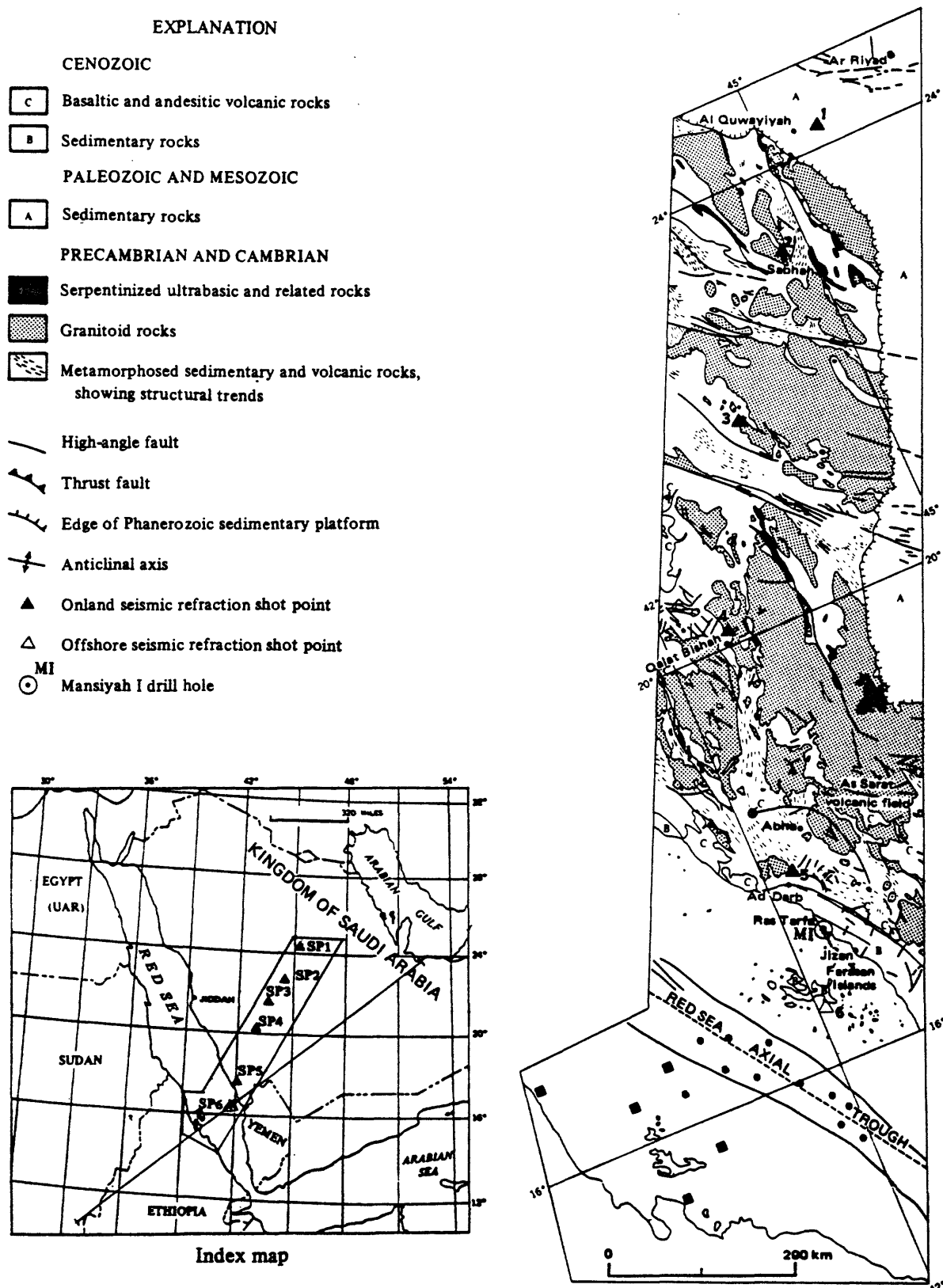


Figure 1.—Generalized geologic map showing the locations of the shot points of the 1978 seismic deep-refraction line (numbered points) and the locations of other heat-flow data points on the shelf (solid squares) and Red Sea (solid circles) areas (Girdler and Evans, 1977). Geologic data are from Brown (1972). The location of the topographic profile of figure 4a is shown on the index map. Dashed line in the Red Sea is an arbitrarily defined axis of the deep-water trough, chosen as a single straight line through the deepest water south of lat 20° N.

Table 1.--Heat-flow estimates from drill holes at shot points 1, 2, 3, 4, and 5, along the seismic refraction line, Kingdom of Saudi Arabia

Shot point locality	Latitude (north)	Longitude (east)	Altitude (meters)	Depth range (meters)	Thermal conductivity (mcal cm ⁻¹ s ⁻¹ °K ⁻¹)	Geothermal gradient (°K km ⁻¹)	Heat flow (HFU)	Geologic unit
1	26°16'12"	45°35'57"	692	43-70	6.28 +0.72	14.74 + 1.89	0.93 +0.16	Sudair Shale
2	23°17'28"	44°40'55"	887	17-69	7.80 +0.78 11.00 +1.10	10.28 + 0.15 8.22 + 0.50 ¹	0.80 +0.08 0.90 +0.11 0.85 +0.07	Greenschist Granite Average
3	21°56'44"	43°34'16"	946	21-62	6.23 +0.62	13.04 + 0.50 ¹	0.81 +0.09 1.00 +0.12 1.00 +0.12	Metabasalt Granite Accepted value ²
4	20°05'13"	42°39'04"	1144	9-58	5.73 +0.57 8.57 +0.86	-- -- 12.43 + 0.64	-- -- 1.07 +0.12	Metadiorite Granite
5	17°46'36"	42°20'47"	179	21-58	10.10 +2.00	18.28, 19.80 ³ + 2.00	2.00 +0.44	Phyllite

¹ Assumed value.

² Three-dimensional heat flow assumed to account for low value in metabasalt.

³ Value of 19.80 is terrain-corrected value.

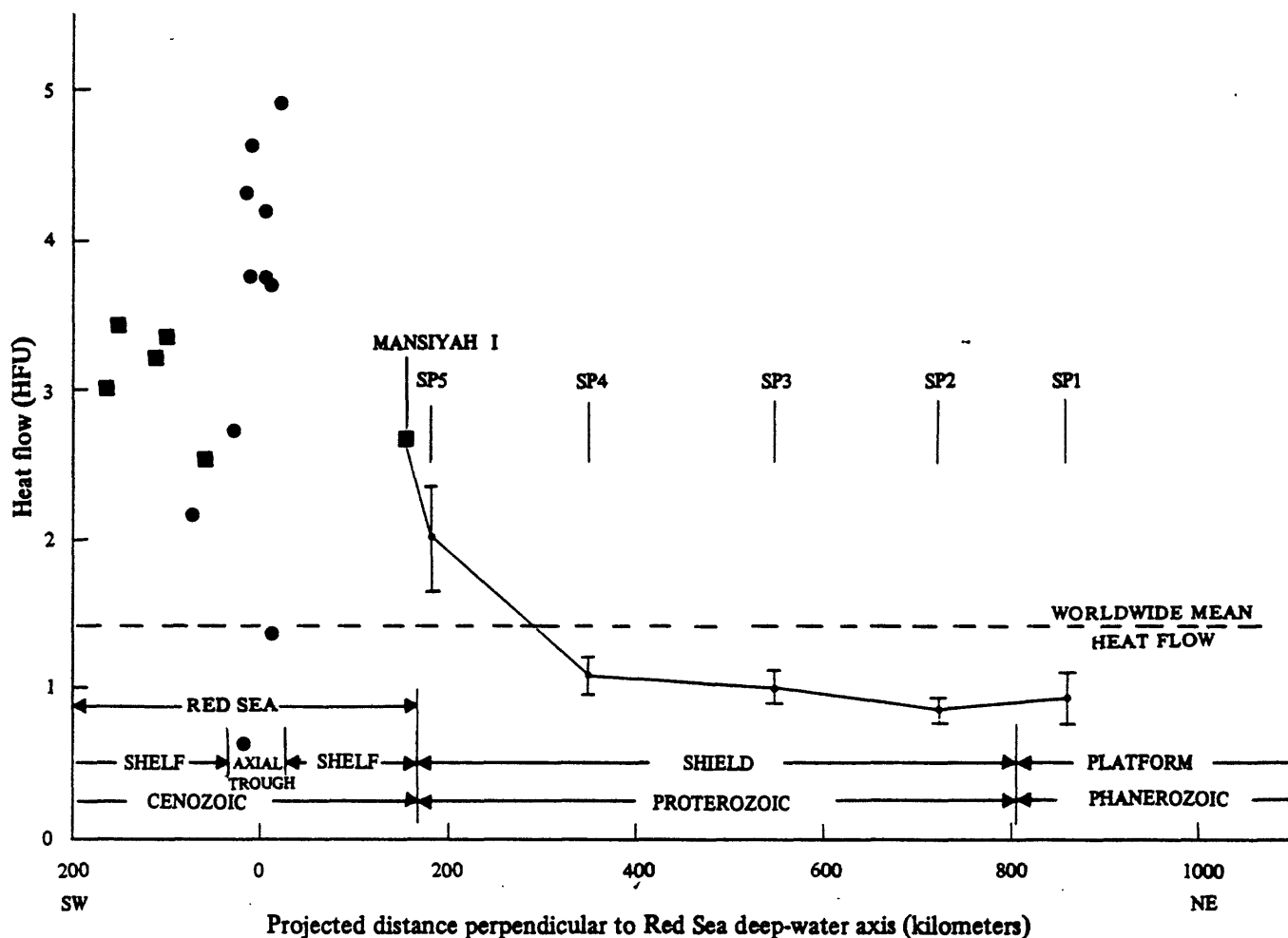


Figure 2.—Plot of heat-flow values as a function of distance from the Red Sea deep-water axis shown in figure 1. Heat-flow data for points other than SP1, 2, 3, 4, and 5 are from Girdler and Evans (1977). One HFU is $1\text{E-6 cal cm}^{-2}\text{s}^{-1}$ or 0.041868 Wm^{-2} . Points in the Red Sea (square symbol) are observations on the shelf area; others (circle) are observations in water deeper than 1 km.

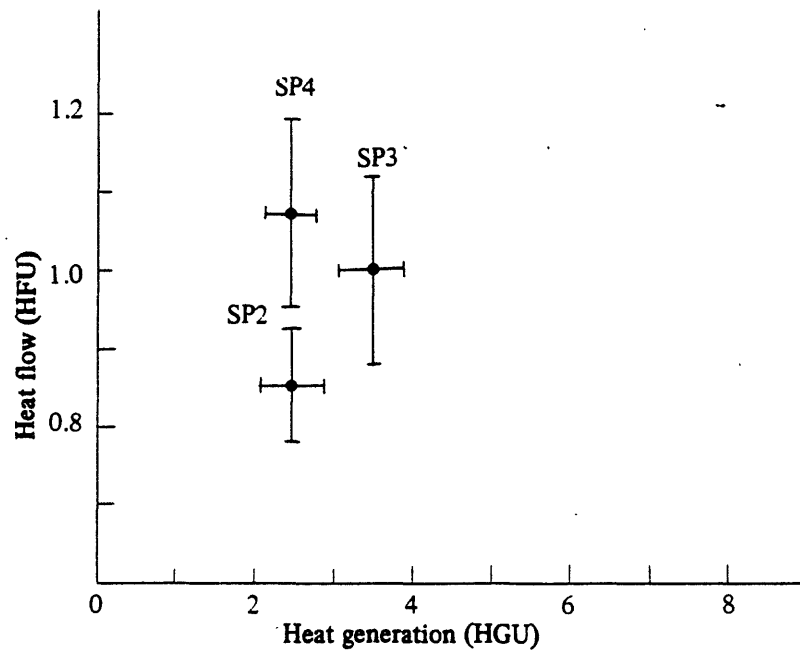


Figure 3.—Plot of heat flow as a function of heat generation for three plutonic rocks of the Arabian Shield (SP2, metagranite and metatonalite; SP3, granite; SP4, granite gneiss). Note the apparent lack of a linear relation. One HFU is $1 \text{ E-6 cal cm}^{-2} \text{ s}^{-1}$, or $4.1868 \text{ E-2 Wm}^{-2}$; one HGU is $1 \text{ E-13 cal s}^{-1} \text{ cm}^{-3}$ or $4.1868 \text{ E-7 Wm}^{-3}$.

This work on which this report is based was carried out as part of a cooperative agreement between the U.S. Geological Survey (USGS) and the Saudi Arabian Ministry of Petroleum and Mineral Resources. H. R. Blank and D. L. Schmidt of the USGS contributed substantially to the structural models described in this work.

A MODEL FOR THE LITHOSPHERE OF THE SOUTHERN RED SEA AND ADJOINING ARABIAN PENINSULA

The Arabian Peninsula, Red Sea, and that part of eastern Africa comprising Egypt, Sudan, and Ethiopia form a broad, approximately symmetrical, rifted zone of uplift, whose axis lies along the Red Sea. This zone is about 2,800 km wide, and the maximum observed uplift is along the margins of the Red Sea. The amount of uplift along the Red Sea escarpments increases southward, from about 2 km in northern and central Saudi Arabia to more than 3 km in southern Saudi Arabia and Yemen. From the summits of the escarpments, the land surface generally dips gently away from the Red Sea to lower altitudes, reaching sea level on the Arabian side at the Arabian Gulf (fig. 4a). The approximate symmetry of the uplift is evident if one ignores the plateaus of Tertiary volcanic rocks on the African half of this particular profile. I restrict the remainder of my discussion to the Arabian side of the profile, from the deep-water axis of the Red Sea northeastward, assuming for my purposes that the system is symmetrical about this axis.

Figure 4b is an average topographic profile from the Red Sea axial trough to the Arabian Gulf showing generalized geochronological relations (Brown, 1972). From the Arabian Gulf, southwestward along the profile, one passes from Quaternary deposits through progressively older sedimentary rocks of the Arabian Phanerozoic platform, which are essentially uniformly stratified and dip about 1° E. or NE. (Powers and others, 1966). The outcrop of the base of the Phanerozoic rocks is at an altitude of about 700 m, and the metamorphic and igneous rocks of the Arabian Shield (Precambrian) are to the southwest. The Shield rocks are capped by Tertiary basalts of the As Sarat volcanic field at the top of the escarpment and by scattered erosional remnants of the basal part of the Phanerozoic section. At the foot of the escarpment, at an altitude of about 200 m, the Precambrian rocks are in direct contact with a narrow belt (about 15 km wide) of Tertiary sedimentary and igneous rocks; in places along this contact, the Precambrian rocks are overlain by sedimentary rocks of Cambrian to Jurassic age. Farther to the southwest, Quaternary surficial deposits form a coastal plain that is approximately 40 km wide. Seaward, the shallow Red Sea shelf (<200 m water depth) is about 120 km wide. The Red Sea axial trough, approximately 30 km in half width and about 1 km in water depth, completes the profile.

From evidence in the sedimentary record (Powers and others, 1966; Gillman, 1968; Madden and others, 1980; Hadley, 1980; Hadley and Fleck, 1980a, b), it appears that regional uplift has taken place since Oligocene time and is intimately related to Red Sea rifting and sea-floor spreading. Although the Phanerozoic platform has been a depositional basin since Cambrian time (illustrated in fig. 4b), the Shield has been a relatively level, stable, and positive feature throughout this period;

lat 10.4°N., long 34.1°E.

lat 23.95°N., long 52.1°E.

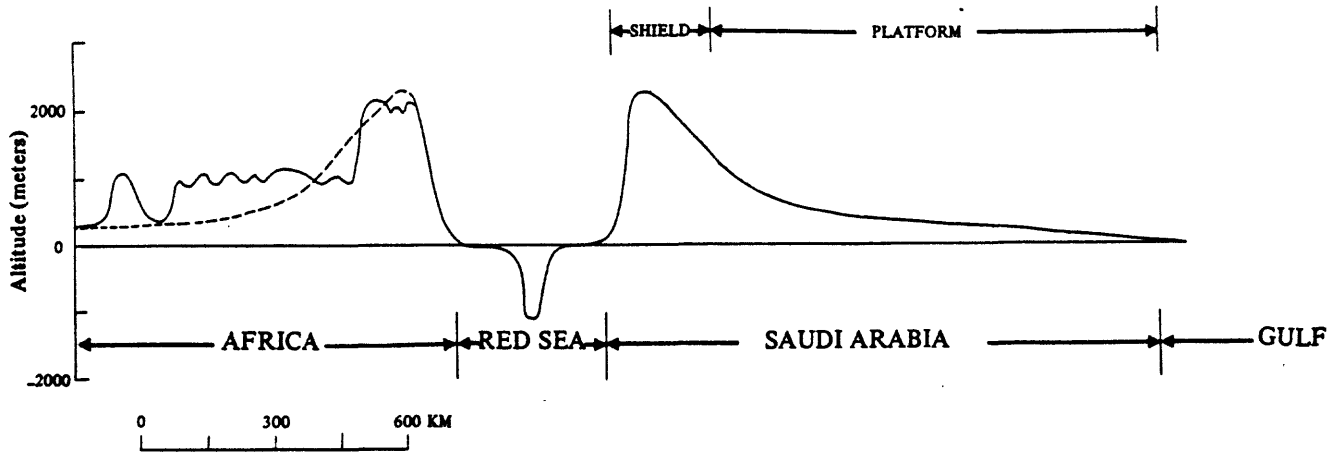


Figure 4a.—Generalized topographic profile for the southern Arabian-Red Sea-East Africa area, along the profile shown on the index map of figure 1. The dashed line on the African side is a reflection of the Arabian portion of the profile. Topographic information is taken from *The Times Atlas of the World* (Bartholomew and Son, Ltd., 1977, plate 27).

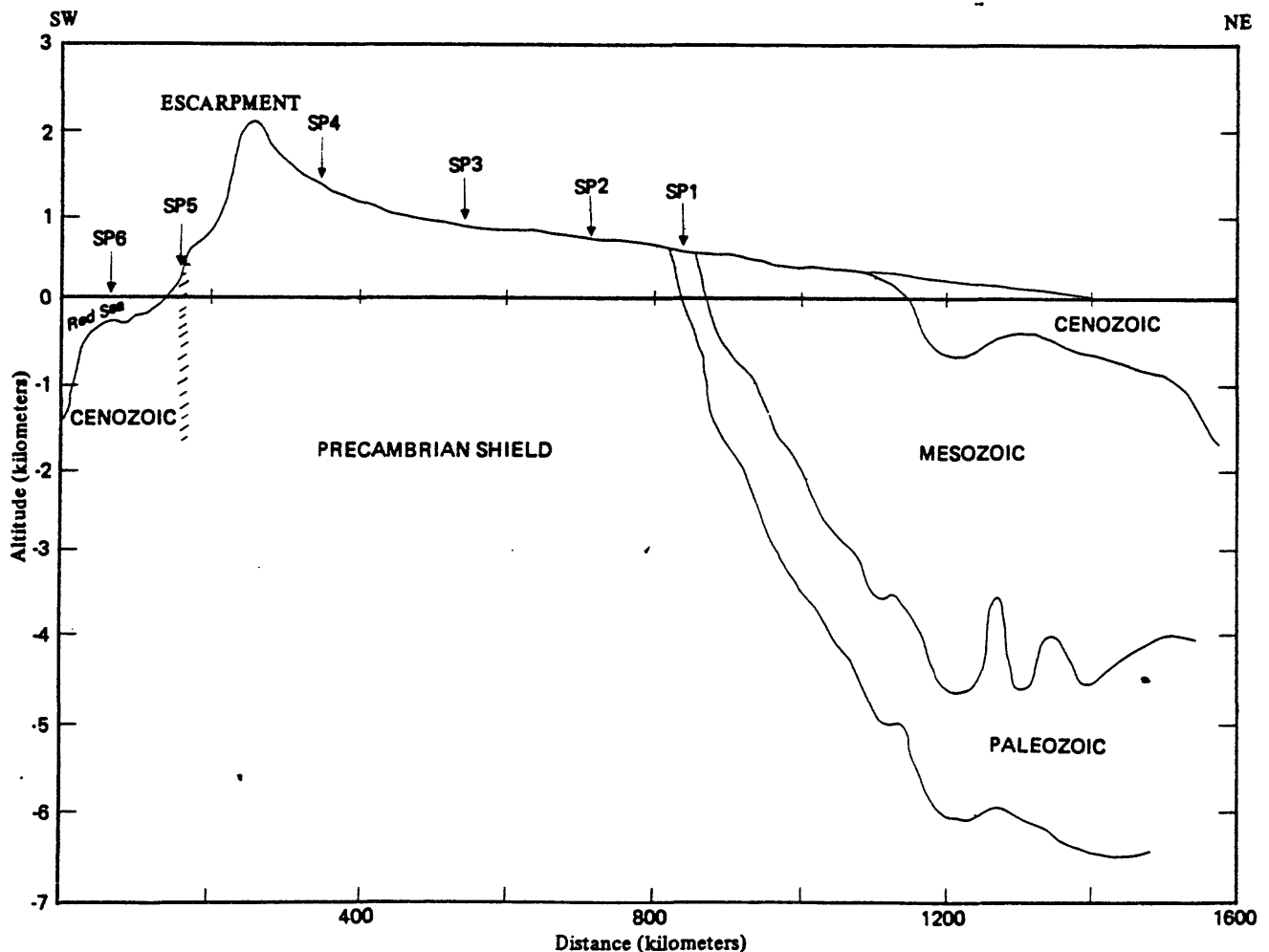


Figure 4b.—Average topographic and generalized geochronological profile for southern Saudi Arabia as a function of distance from the Red Sea deep-water axis (fig. 1). Profile is an average of seven profiles, spaced 100 km apart, northward from 100 km south of shot point 6. Geochronological-geological data from Brown (1972); topographic profiles from U.S. Geological Survey (1972). Vertical exaggeration about $\times 120$. Hatchured symbol marking the boundary between Cenozoic and Precambrian Shield rocks denotes the complex transition zone where the crust changes from continental character to the east to oceanic to the west.

at most it has undergone only small-scale uplift, subsidence, transgression by shallow seas, and deposition of sedimentary rocks (Powers and others, 1966). During Miocene-Pliocene and Quaternary times, however, tilting of the Shield down to the east resulted in sedimentation on the platform area that reflects increased erosional activity on the Shield (Powers and others, 1966). From the sedimentary record of this period, it appears that uplift of the Shield may have been continuous, with several superimposed episodes of more rapid uplift.

Additional evidence for the timing of the initiation of uplift can be found in the lateritic soil profile beneath the As Sarat volcanic field near the top of the escarpment (fig. 1). A 20- to 30-m-thick laterite is preserved beneath the volcanic flows on a nearly flat Precambrian surface at an altitude of about 2,300 m (Overstreet and others, 1977). The laterite is thought to be late Oligocene in age, and the lowermost overlying basalt flows have been dated at 29 Ma (mega-annum) by K-Ar methods (Brown, 1972). The lower flows also show evidence of lateritic weathering, and, together with the absence of a well-developed erosional surface on the laterite, these relations suggest that the laterite was still forming when the lava flows were erupted (Overstreet and others, 1977). It seems doubtful that the laterite could have survived erosion in the present terrain of high relief, and I conclude that the uplift must have occurred after the eruption of the As Sarat lavas, whose uppermost flows are dated at 25 Ma (Brown, 1972).

To the north, near At Taif, Paleocene vertebrate fossils have been found in coastal deposits, which have been uplifted since Oligocene time to a present-day altitude of about 1,200 m (Madden and others, 1980). The geologic record in this area suggests two phases of rapid uplift, one during Miocene time and another in Pliocene or younger time.

This evidence suggests that the Shield was a relatively flat surface near sea level throughout early Tertiary times. Broad regional tilting associated with the rifting of the Red Sea uplifted the Arabian Shield and Phanerozoic platform progressively more to the southwest, exceeding 3 km of uplift in southwestern Saudi Arabia. The uplift began in Miocene time and has continued to the present. During this time, the rate of uplift has increased at least twice. Understanding this regional uplift in the context of Red Sea rifting constitutes one of the fundamental problems in deciphering the Cenozoic geologic history of the area. I do not undertake this task here; instead, I shall be satisfied with a few relevant observations.

Evidently the mechanism causing the uplift must involve the mantle, as suggested by the large horizontal distances over which the uplift has occurred and the relatively low strength of the crust over such distances. In view of the association of the uplift with Red Sea rifting, one mechanism might be the replacement of large volumes of "cold" mantle by "hot" in some sort of upwelling centered beneath the Red Sea rift accompanied by lateral spreading as a consequence of a mantle convection system.

A working hypothesis is that in late Cretaceous or early Tertiary time, the time of earliest movements on the Dead Sea Rift (Girdler and

others, 1980), instabilities in the asthenosphere led to the onset of mantle convection, with upwelling along the present-day Red Sea axis and subduction along the present-day Zagros fold belt. The time scale for full development of this convective system is unknown; surface manifestations at the Red Sea axis began with volcanism about 30 Ma ago (As Sarat volcanic field), whereas the major folding and mountain-building in the Zagros was in Pliocene time (5 to 1.8 Ma ago) (Powers and others, 1966). Thus, the Red Sea-Arabian plate spreading system appears to be very young, perhaps not yet fully developed. The asthenosphere below both the Red Sea and at least the western part of the Arabian plate is characterized in this model by flow from the Red Sea axis toward the Zagros mountains, which systematically moves "cold" asthenosphere to the northeast. In view of the scale of the system, it is not unreasonable to suppose that accretion (Lachenbruch and Sass, 1978) of some of this asthenospheric material is occurring in the lithosphere beneath the Red Sea and the western part of the Shield to accommodate the extension.

In this conceptual model, regional uplift is caused by the progressive replacement of cool upper asthenosphere and lower lithosphere by higher temperature material, which leads to a lower average density for the lithosphere-asthenosphere column and hence to uplift to maintain isostatic balance. The detailed demonstration that such a model fits constraints imposed by the available heat-flow, gravity, and seismic data is beyond the scope of this paper and will be presented elsewhere (Gettings and Blank, unpub. data). This model of the transitional process from a stable continental condition to an actively spreading oceanic ridge system has as its principal feature the development of mantle convection beneath both the Red Sea and the Arabian plate. Therefore, the process beneath the Arabian plate can be viewed as a northeastward-progressing heating event, which because of the thermal inertia of the continental crust is presently observable at the surface. This part of the system thus differs from oceanic ones (McKenzie, 1967; Sclater and Francheteau, 1970), in that it is heating up rather than cooling down. Because the time constant for approach to steady state of a normal continental crust (Lachenbruch and Sass, 1977) is of the same order as the flow processes in this model, steady-state models may be of limited applicability. Thus thermal models of ocean-floor topography (McKenzie, 1967; Sclater and Francheteau, 1970; Davis and Lister, 1974; Parsons and Sclater, 1977), which might be used to test the model, may not be applicable without modification. I note, however, that these models (see, for example, Sclater and Francheteau, 1970) do yield differences in altitude of about 3 km over comparable horizontal distances and thus demonstrate that temperature differences in the lower lithosphere-upper asthenosphere of the magnitudes expected between a hot oceanic and a cool continental system produce the correct order of magnitude of elevation difference.

To investigate further whether reasonable variations of mantle parameters might yield the right order of magnitude of uplift, a lithospheric column having a temperature profile characteristic of an oceanic spreading environment can be compared with the same column having a temperature profile characteristic of a stable continental environment; the two columns are assumed to be in isostatic equilibrium with each other.

The density of the columns is a function of composition, temperature, and depth, which I approximate by a bilinear function of temperature and pressure. By considering the same column under two different thermal regimes, I minimize the effects of composition and pressure variations. The two columns now are of the same total mass down to a depth H in the mantle where the two geotherms coincide. However, the top of the column with the oceanic geotherm projects h kilometers above the other because of its higher average temperature. If the temperature variations in the upper h kilometers of the oceanic column are ignored,

$$h = \beta \int_{T_0}^T \Delta T(z) dz \quad (1)$$

Note that the function $\Delta T(z)$ refers to the difference between the oceanic and continental geotherms and that h is independent of the average column density in this approximation. To arrive at an actual value for h , the continental and oceanic geotherms of Froidevaux and others (1977, p. 242) are used to a depth of 450 km where they merge. The numerical evaluation of equation (1), using a digitization interval of 50 km and a ΔT value of $1.5E-5$ (Skinner, 1966), yields $h=1.2$ km as a lower bound on the uplift because the oceanic geotherm used is for oceanic crust in older (cooler) ocean basins (Froidevaux and others, 1977). I conclude that lateral mantle-density variations in the asthenosphere and lithosphere caused by mantle upwelling into the Red Sea spreading system are at least capable of providing the observed uplift; further, the scale of the system is large enough to provide for regional uplift, rather than uplift just along the immediate vicinity of the Red Sea axis.

As to the age and extent of the oceanic crust in the Red Sea basin, there is little question that the central deep-water trough of the Red Sea is an active sea-floor spreading center, spreading at a half-rate of about 0.8 cm y^{-1} (see, for example, Hall (1980) and references therein). Further, this spreading seems to have been active for about the last 5 Ma.

Although the shelf was initially interpreted to be thinned continental crust (for example, Coleman and others, 1977), combined geologic, geophysical, and geochemical evidence (Girdler and Styles, 1974; Blank and others, 1975; Gettings, 1977; Greenwood and Anderson, 1977; Blank and others, 1979a; Coleman and others, 1979; Hall, 1980) suggests that the entire shelf and coastal plain from the edge of Precambrian outcrop seaward are underlain by oceanic crust beneath the Tertiary sedimentary rocks. One of the most compelling pieces of evidence is the palinspastic reconstruction of Greenwood and Anderson (1977), which demonstrates that closing the Red Sea at the boundaries of exposed Precambrian rocks not only results in a good fit but unites structural and lithologic trends across the closure as well.

The geomagnetic stratigraphy of the older oceanic crust (termed stage 1 or phase 1 spreading by Girdler and Styles, 1974) and the geologic and geochronologic evidence (Gillmann, 1968; Coleman and others, 1979) indicate that the oceanic crust beneath the shelf and coastal plain was probably created 30-15 Ma ago at a half-rate of about

2 cm yr⁻¹ (Hall and others, 1977). Stage 1 spreading resulted in the creation of about 160 km of crust, and stage 2 spreading has added approximately 30 km to the width of the Red Sea basin from the deep-water axis eastward, for a total half-width of about 190 km. As noted above, stage 2 spreading began about 5 Ma ago.

During Miocene time, a series of marine sedimentary rocks more than 4 km thick, including a thick evaporite sequence, was deposited on stage 1 crust (Gillman, 1968). Some of these rocks have been uplifted above sea level on the coastal plain west of the edge of the oceanic crust. Presumably, Miocene subsidence in response to sediment loading was followed by uplift at the margin of the oceanic crust. In addition, tectonism due to salt flowage is presently active and has resulted in the emergence of the Farasan Islands.

The seismic deep-refraction profile carried out in 1978 (Blank and others, 1979b) provided the data for construction of a crustal section through the area shown in figure 1. Preliminary analysis (Blank and others, 1979b) indicated that the crust in the Shield area is approximately 40 km thick and is composed of two layers of equal thickness. This crust thins drastically to a thickness of about 15 km beneath the coastal plain and Red Sea shelf near shot point 5 (fig. 1). The schematic crustal cross section (fig. 5) is derived by analysis of first-arrival times using the preliminary seismic record sections included in Blank and others (1979b). The gravity profile (fig. 5) was also used to constrain the model; within the uncertainties of density contrast that result from uncertainties about average velocities and their conversion to density values, the model fits the gravity data southwest of shot point 3 (fig. 1). The rock compositions in the Shield area of figure 5 were deduced from the models of Schmidt and others (1978) and were considered in the conversion of velocities to densities (see Nafe and Drake, 1968). The section has been projected to a profile perpendicular to the deep-water axis of the Red Sea west of the Farasan Islands (fig. 1). West of shot point 5, the drill-hole data at Mansiyah I (Gillman, 1968) help constrain the solutions for the oceanic crust. The section shown in figure 5 differs somewhat from that of Le Pichon and others (1976, p. 173; see also Worzel, 1974). Velocities in layer 1 (sedimentary layer) are quite high (4.5 km s⁻¹), due at least in part to the high proportion of halite and anhydrite (>1,500 m, Gillman, 1968) in the section. The layer 2 velocity of 6.1 km s⁻¹ is in the high end of the range, and the layer itself is about twice the average thickness. The layer 3 velocity of 6.7 km s⁻¹ is near the mean, and this layer is also significantly thicker than the average. Mantle velocity is average for that beneath oceanic crust, and indeed, mantle velocities are average, within uncertainties, for the entire section including the Shield area. This interpretation of the seismic data is only tentative. No weathering corrections or allowances for delays due to surface lithologic variations have been made, and because large segments of the profile traverse areas of unconsolidated cover, particularly between shot points 5 and 6 (coastal plain) and between shot points 3 and 4, such corrections may be substantial. Also, no allowance has been made for topographic relief, which is about 2,000 m between shot points 4 and 5. The uncertainties in the depths and thicknesses of the layers are probably of the order of ±15 percent.

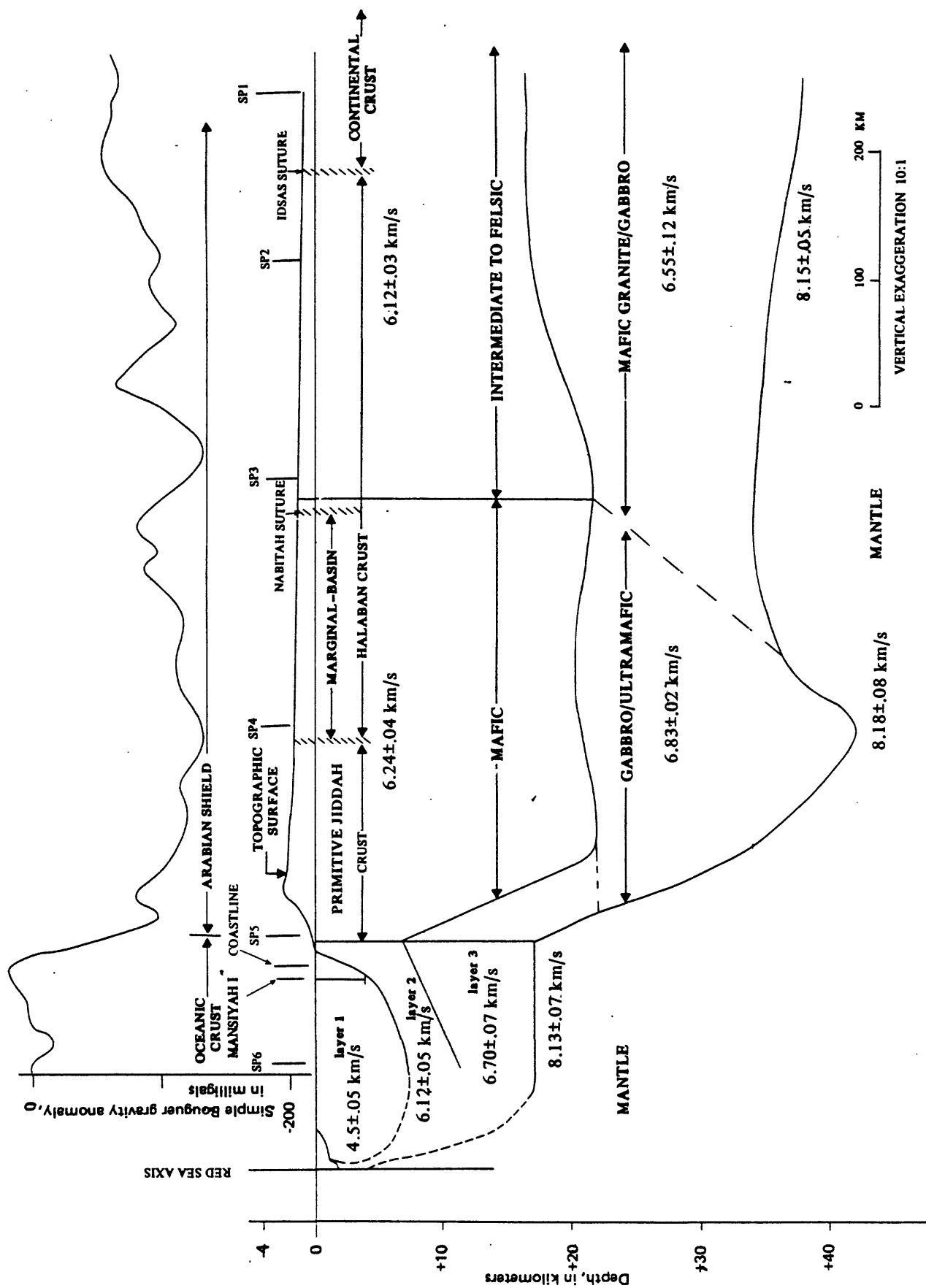


Figure 5.—Schematic crustal cross section for the southwestern Saudi Arabia-southern Red Sea area derived by analysis of first arrivals on the preliminary seismic deep-refraction record sections contained in Blank and others (1979b) and the Bouguer gravity anomaly profile by Gettings. Geologic information from Schmidt and others (1978). Section is projected perpendicular to the Red Sea axis shown in figure 1.

Given the wide spacing of the heat-flow data (fig. 2), the details of the crustal profile are unimportant; for my purpose, the section is considered to be composed of three horizontally layered provinces. In the deep-water portion of the Red Sea, where new oceanic crust is being formed, a thin sedimentary layer is underlain by a hot crust 15 km or less in thickness, which is in turn underlain by an actively upwelling mantle. This region is characterized by a heat flow of about 4 HFU. On the Red Sea shelf and coastal plain, older oceanic crust is overlain by a 4- to 7-km-thick blanket of Tertiary shales, sandstones, and evaporites, which feather out at the continental margin. This sedimentary province is characterized by a heat flow of about 3 HFU. On the Shield, the crust is approximately 40 km thick and evidently becomes more mafic with depth. This province is characterized by a heat flow of about 1 HFU.

Shot point 5 is the only data point near a major lateral discontinuity, and interpretation of the heat flow at this locality must take into consideration the nearby oceanic plate. At the other data points, interpretations are confined to one-dimensional models, most of which are time-independent. The thermal time constants (Lachenbruch and Sass, 1977) for oceanic provinces justify these assumptions for the Red Sea part of the profile, especially considering the sparseness of data in the heat-flow profile. For the Shield, the thermal time constant may be of the same order as the asthenosphere-lower lithosphere thermal processes involved, and therefore the use of steady-state models is questionable. Nevertheless, steady-state models have been applied to this province as well because of the considerable insight gained from them and because the data distribution and uncertainties do not justify the additional complexity introduced by time-dependent models.

GEO THERM ESTIMATES FOR THE ARABIAN SHIELD

At shot points 2, 3, and 4, the heat-flow measurements were made in granitoid intrusive rocks (fig. 1). If it is assumed that the radiogenic heat sources are distributed in an exponentially decreasing manner with depth, these heat-flow measurements, together with estimates of heat production, allow the construction of a geotherm at each site. I model the crust as a layer of uniform thermal properties and assert that the surface heat flow is the sum of two terms: a constant component, q_m , from the base of the crustal layer; and a variable component, q_c , arising from the exponential distribution of radiogenic heat production in the crustal layer. In most models the heat flow at zero heat production, termed the "reduced heat flow", is equivalent to q_m . Thus, at the measurement site (Lachenbruch, 1970):

$$A(z) = A_0 e^{-z/D}, \quad (2)$$

$$q(z=0) = q_m + DA_0, \quad (3)$$

and

$$\theta(z) = [q_m z + D^2 A_0 (1 - e^{-z/D})] / K \quad (4)$$

for the crustal heat production, surface heat flow, and temperature at depth z . In these equations, z is the depth below the surface, A_0 is the heat productivity at the surface, D is the decrement (units of length), and K is the thermal conductivity taken here to be $0.006 \text{ cal-cm}^{-1}\text{-s}^{-1}\text{-K}^{-1}$. The decrement D , which characterizes the rate of decrease of $A(z)$ with depth, is presumed to be a characteristic and generally constant parameter for a region. Most estimates of D for Precambrian shields are about 10 km (Pollack and Chapman, 1977), the value which I adopt here. Having measured A_0 and $q(z=0)$, I arrive at an estimate of q_m using equation (3) and calculate a temperature profile (geotherm) for the site using equation (4). The results of this exercise are shown in figure 6.

In order to evaluate the effects of erosion and uplift on the heat-flow observations at shot points 2, 3, 4, and 5, I turn again to the Tertiary geologic record. The amount of erosion from the top of the escarpment eastward since mid-Miocene time seems on the average to have been rather small as indicated by the following evidence. In the area of the As Sarat volcanic field, basal flows of the field lap onto and over erosional remnants of the Cambrian-Ordovician Wajid Sandstone, which overlies Precambrian basement (Coleman and others, 1977; Anderson, 1979); this evidence indicates these outliers have not been greatly eroded in the last 29 Ma. In this area, relief on the Precambrian surface between basal As Sarat flows and nearby wadis is about 100 m. On the east side of the As Sarat volcanic field, erosion has been less than on the west and is a few tens of meters (J. Whitney, oral commun., 1981). In the Hamdah area, about 150 km to the northeast, a silicified laterite is found on isolated ridgetops, and, if this laterite is the same age as that below the As Sarat basalts, the erosion in this area since mid-Miocene time has been about 70 m (J. Whitney, oral commun., 1981). The topographic relief on the Shield in the region of shot points 2, 3, and 4 is about 300 m, which may be regarded as a maximum limit for the amount of erosion.

Northwest of shot point 5, on the west side of the escarpment, basal basalts of the Al Birk volcanic field, which rest on Precambrian rocks, have been dated by K-Ar techniques at about 12 Ma (Hadley, 1975; Brown, written commun., 1980). To the east of this volcanic field and north of shot point 5, isolated cones and flows, 5 Ma old, overlie Precambrian rocks (Brown, written commun., 1980). The relief of the surrounding Precambrian terrane is 100 m or less. South of shot point 5, near Jabal at Tif, Quaternary basalts, 1 Ma old or less (Coleman and others, 1977), rest on Precambrian rocks having a few tens of meters of relief. I conclude that erosion at shot point 5 has been 100 m or less, at least during the last 1 Ma and probably during the last 13 Ma.

Basal flows of Harrat Rahat north of Jiddah, which flowed down valleys in Precambrian rocks from the top of the escarpment to nearly sea level, have been dated by K-Ar methods at 13-12 Ma (Brown, written commun., 1980). Geologic mapping (Smith, 1980; Gilboy and Skiba, unpub. data) shows no faults cutting these flows. In contrast, the As Sarat volcanic field (29-25 Ma old) is extensively faulted (Anderson, 1979). These relations suggest that the major uplift and formation of the escarpment occurred in the interval 25-13 Ma ago.

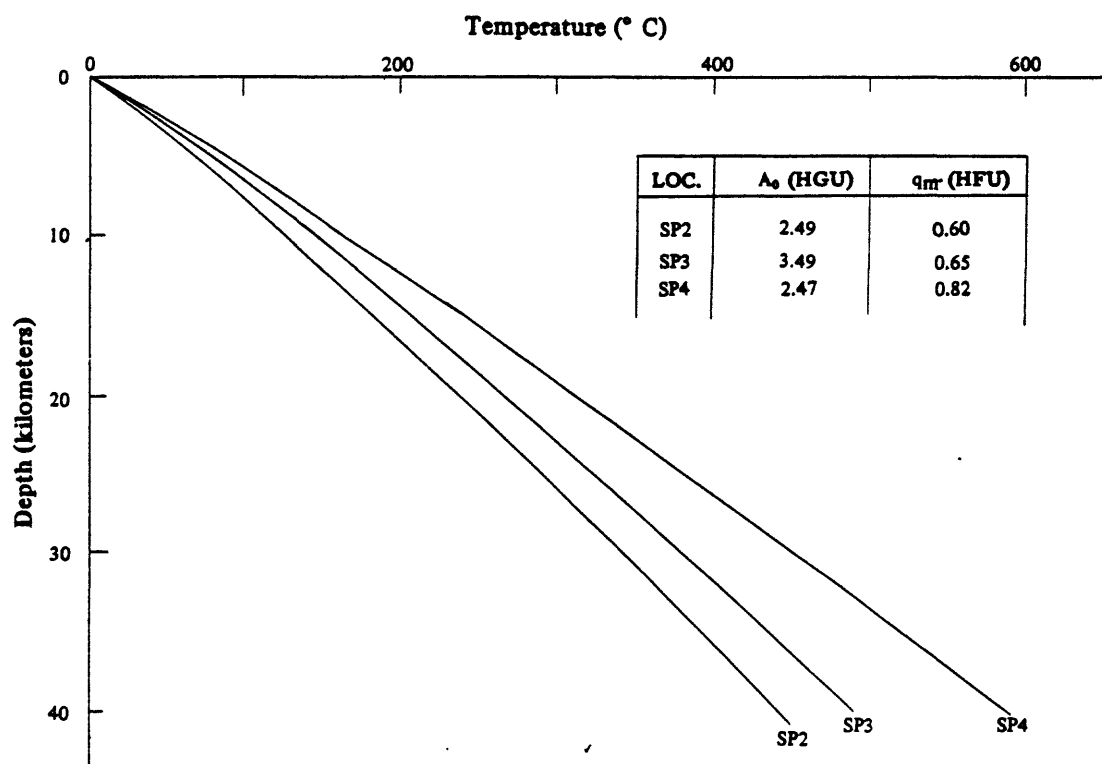


Figure 6.—Geotherm estimates for the Arabian Shield at shot points 2, 3, and 4. Estimates are based on the assumption of an exponentially decreasing distribution of radiogenic elements with depth. Uncertainties in the parameters give a probable uncertainty at 40 km depth of about $\pm 60^\circ\text{C}$, so that SP2 and SP3 geotherms are essentially identical, and SP4 attains a significantly higher temperature. A thermal conductivity of $0.006 \text{ cal cm}^{-1} \text{ s}^{-1} \text{ }^\circ\text{C}^{-1}$ was used, and a heat-source distribution decrement of 10 km was assumed.

The effects of 100 and 300 m of erosion over 1 million years were evaluated using the formulae of Jaeger (1965) and found to be well within the uncertainties of the heat-flow measurements at shot points 2, 3, 4, and 5. The effects on the heat-flow measurements of uplift 13 Ma ago or more, which are generally less important than those of erosion (Benfield, 1949), are negligible at all five sites.

Late Pliocene and Pleistocene climatic variations have produced significant effects on observed heat-flow values, especially in shallow drill holes (Birch, 1948; Jaeger, 1965). Pluvial periods lowered the mean surface temperature and caused the presently observed surface heat flow to be lower than the actual flux of heat from within the Earth. Although studies of Pliocene and Pleistocene climatic variations in the Arabian Peninsula are few, some generalizations can be made (Hotzl and Zotl, 1978; J. Whitney, oral commun., 1981). The last long, intense humid phase, in which a river system and associated geomorphic features developed, occurred in late Pliocene and early Pleistocene times, 3.5 to 1.2 Ma ago. In this period, the mean annual temperatures throughout the Peninsula might have been about 5°C lower than those of today.

During the Pleistocene, the only humid phase of any consequence so far documented was from 32,000 to 22,000 years ago, when lakebed deposits and similar features formed. Age determinations of ground water from major aquifers fall in this period and thus also indicate increased precipitation. Pollen studies suggest that this period might have been characterized by a lowering of mean temperatures by 2° or 3°C, certainly no more than 5°C. Several more recent humid periods have also been identified, but, because of their very limited preservation in the geologic record, they appear to have been of short duration and to have been balanced by periods of climate similar to that of today.

The effect of these climatic variations on the heat-flow observations was therefore estimated by calculation of the perturbation to the present geothermal gradient caused by two periods in which the mean surface temperature was 5°C lower than at present, one from 3.0 to 1.0 Ma and another from 32,000 to 22,000 years ago. Calculated according to the formulation of Jaeger (1965), this perturbation amounts to a maximum depression of the present geothermal gradient of $0.9^{\circ}\text{K}\cdot\text{km}^{-1}$, which is of the same order as the observational uncertainty in the measured gradients. So, within experimental error, this perturbation results in a systematic increase in heat-flow values at the five shot points of about 0.07 HFU. Because of the small amplitude and systematic nature of the correction, it has not been applied to the heat-flow values given here.

Allowing for reasonable variations in the parameter values, the uncertainty in the temperature profile at a depth of 40 km is about $\pm 60^{\circ}\text{C}$. It appears, therefore, that shot points 2 and 3 have similar geotherms, whereas shot point 4 has a demonstrably higher geotherm. For a crust 40 km thick with a thermal diffusivity of about $0.008\text{ cm}^2\cdot\text{s}^{-1}$, the time constant for approach to steady state (Lachenbruch and Sass, 1977), which is a measure of the time needed to "feel" at the surface ($z=0$) a thermal pulse at the base of the crust, is

about 15 Ma. I would expect that if there had been thermal disturbances at the base of the crust during the last 30 Ma that correspond to mantle flow associated with Red Sea rifting, their surface manifestations should be detectable and should increase in intensity toward the Red Sea rift. Such seems to be the case, although heat-flow measurements from deeper holes and of corresponding higher reliability are needed to definitely establish this relationship. The lack of a linear relationship between heat flow and heat production (fig. 3) is also indicative of regions undergoing active tectonism (Lachenbruch and Sass, 1977; Smith and others, 1979). Given our present state of knowledge, a geotherm estimate for shot point 1 would be identical to those for shot points 2 and 3.

SOME THERMAL MODELS FOR THE OCEANIC LITHOSPHERE

I now attempt to provide some insight into the thermal regime of the oceanic lithosphere in the Red Sea rift system by evaluating some simple models and limiting cases. Because I shall now permit dynamic systems as well as static ones, I have more parameters for essentially the same number of observations and a corresponding decrease in the probability of constructing a realistic model.

For the present actively spreading Red Sea trough, I find simple models of accreting slabs adequately predict the high heat flow (4 HFU) observed. For the Red Sea shelf and coastal plain, which are characterized by a heat flow of about 3 HFU, several possible models give varying results. Because most shelf measurements that establish the 3-HFU level are from the western side of the Red Sea, for which much less geological and geophysical information is available than for the eastern side, I shall weight the single measurement at Mansiyah I (Girdler, 1970) heavily and use 2.7 ± 0.3 HFU as representative of the heat flow on the eastern shelf.

Finally, I shall discuss some of the implications of the nearby oceanic crust on the heat flow at shot point 5.

Estimates of parameter values

Thermal conductivity and diffusivity

Following Lachenbruch and Sass (1978), I define the base of the lithosphere in a thermal sense by means of the intersection of the geotherm with the basalt dry solidus, which I approximate by:

$$\theta_m(z) = \theta_0 + mz, \text{ where} \quad (5)$$

$$\theta_0 = 1050^\circ\text{C}, m = 3^\circ\text{C km}^{-1}.$$

At $z=R$, which is the base of the lithosphere, $\theta(R) = \theta_m(R)$. These parameters are chosen to approximate the peridotite solidus as well as the basalt dry solidus (Lachenbruch and Sass, 1978), so that below R a substantial fraction of liquid may exist if the mantle material has the

appropriate composition. Estimates of R for oceanic crust near active spreading centers range from 30 to 75 km (Pollack and Chapman, 1977); thus temperatures at the base of the lithosphere are likely to be near 1,200°C. Since the surface temperature is near 0°C, I base my estimates of thermal properties for the majority of the lithosphere column on temperatures of about 600°C to arrive at appropriate average values for the models.

At 600°C, thermal conductivities (Murase and McBirney, 1973) for lherzolite are about $8.5\text{E-}3 \text{ cal-cm}^{-1}\text{-s}^{-1}\text{-}^{\circ}\text{K}^{-1}$ and for dunite about $7\text{E-}3 \text{ cal-cm}^{-1}\text{-s}^{-1}\text{-}^{\circ}\text{K}^{-1}$. For gabbro and basalt at about 100°C, conductivities of about $3.5\text{-}4.0\text{E-}3 \text{ cal-cm}^{-1}\text{-s}^{-1}\text{-}^{\circ}\text{K}^{-1}$ are reasonable, for shale $6\text{E-}3$, and for anhydrite and halite $12\text{E-}3$ (Clark, 1966). For my purposes, I assume a lithosphere composed of 30 to 40 km of lherzolite or dunite, overlain by 10 to 15 km of basalt and gabbro, and capped by 2.5 km of shale and 1.5 km of halite and anhydrite. For steady-state heat flow in a composite slab such as this, the average conductivity is given by the total thickness divided by the thermal resistivity (Carslaw and Jaeger, 1959, p. 93). Thus, for the above section, the best estimate of average thermal conductivity is $6.4\text{E-}3 \text{ cal-cm}^{-1}\text{-s}^{-1}\text{-}^{\circ}\text{K}^{-1}$.

For specific heat, I use values of single-mineral specific heats at about 600°C (Kelley, 1960). For all minerals of mafic igneous rocks, which compose most of the section, the specific heats are nearly equal, $0.268\pm 0.03 \text{ cal-g}^{-1}$, and therefore I adopt 0.27 cal-g^{-1} as the average specific heat value.

The weighted average of typical densities for the section is 3.2 g-cm^{-3} . This value yields a thermal diffusivity of $7.4\text{E-}3 \text{ cm}^2\text{-s}^{-1}$.

Spreading velocities and strain rates

As noted above, evidence favors two stages of Red Sea spreading. In the first stage, about 160 km of crust was created in the study area at a rate of about 2 cm y^{-1} , sometime during the period 30 to 15 Ma ago. In the second stage, about 30 km of crust has been created at the rate of 0.8 cm y^{-1} during the last 5 Ma. These rates and widths refer to the eastern half of the Red Sea only; comparable amounts of crust presumably have been produced on the western side as well. For the simplest case, I assume that 190 km half-width of new crust was created in the last 30 Ma, which yields an average rate of 0.63 cm y^{-1} . The two stages of sea-floor spreading apply only to crustal formation and do not necessarily imply cessation of the convective system in the asthenosphere between stages of formation of oceanic crust.

The strain rates are dependent on where one places the eastern limit of horizontal extension. If the As Sarat volcanic field just east of the summit of the escarpment is considered the eastern limit of Tertiary activity, I obtain a strain rate of about 2 percent per Ma; thus I conclude that strain rates in the range of 2 to 4 percent per Ma are reasonable values for this system. This kind of model averages out the

ridge extension across the entire Red Sea shelf. As such, it represents a limiting-case model, as opposed to classical sea-floor spreading, where the strain rate away from the ridge is zero. Distributed strain across the Red Sea shelf and coastal plain could have occurred beneath the sediments, either during the interval between the two stages of active sea-floor spreading or throughout the process. In the latter case, the total amount of spreading would be the sum of the distributed strain and the newly formed oceanic crust. This relationship implies that in stage 1 less than 160 km of crust was formed; this crust was then subsequently extended by distributed strain to 160 km. In such a model variations in the wavelengths of the sea-floor magnetic anomalies would be observable. Distributed extensional strain in the stage 1 crust might not be fully developed in the overlying sediments because it would be at least partly masked by salt flowage in the thick evaporite sequence. There is some evidence of normal faulting in the morphology of the coastal plain (Gillman, 1968), and seismic reflection profiles show a homoclinal flexure beneath the coastal plain (Gillman, 1968; note that in this paper Gillman refers to the boundary zone between the Tertiary and Precambrian rocks as a homoclinal flexure). The picture is complicated by possible faulting associated with salt tectonism; conversely, perhaps the movements of the evaporites are in part caused by faulting associated with distributed extensional strain.

Both the classical ridge-type and the distributed extensional strain-type models were evaluated in order to investigate the limiting heat-flow fields for a combined model such as discussed above.

Radiogenic heat-source distributions

Three distributions of radiogenic heat sources were considered for the oceanic lithosphere; one is the distribution of Pollack and Chapman (1977), in which the upper 10 km of lithosphere contains a constant $0.2 \times 10^{-13} \text{ cal cm}^{-3} \text{ s}^{-1}$ (0.2 HGU; HGU = heat generation unit) with no heat sources below. The other two distributions were taken from Sclater and Francheteau (1970). Both contain a layer 5 km thick, which has a heat production of 1.2 HGU. In one distribution, this layer is underlain by a layer 95 km thick, which has a heat production of 0.03 HGU; in the other, a layer 15 km thick (heat production 0.03 HGU) is underlain by a layer 80 km thick (heat production 0.10 HGU). Because the dynamic models of Lachenbruch and Sass (1978), considered below, require a heat-source distribution that decreases exponentially with depth, the three distributions were converted to exponential distributions that have the same total heat production through the thickness of the lithosphere. For the model of Pollack and Chapman (1977), I arrive at $A_0 = 0.299 \text{ HGU}$ and $D = 7 \text{ km}$ (see equation 2), and for the model of Sclater and Francheteau (1970), I obtain $A_0 = 1.2 \text{ HGU}$ and $D = 10 \text{ km}$ and 30 km , respectively, for $R = 100 \text{ km}$. In any case, given the uncertainties in the data and the relatively small heat productions assumed, the effect of various heat-source distributions turns out to be of second order for this work. A similar observation was also made by Sclater and Francheteau (1970).

As a further complication, the sedimentary section includes thick deposits of shales, which may contain highly variable amounts of radiogenic components eroded from the rocks of the Shield. In view of this situation, the best estimate that can be made of the component of heat flow on the shelf due to radiogenic sources in the lithosphere is probably in the interval of 0.1 to 0.4 HFU; thus, the reduced heat-flow values for this area are in the range of 2.3 to 3.1 HFU.

Static models for the shelf area

I will now attempt to match the observed heat-flow level in the stage 1 oceanic crust with models that ignore sea-floor spreading and thus convective heat transport. For an initial model I apply the formulae of equations 2 through 4 and extend the geotherm until it intersects the solidus (equation 5). These results are shown in figures 7a and 7b as the static case. In fig. 7a, D is 30 km and in fig. 7b it is 10 km, corresponding to the two radiogenic heat-source distributions of Sclater and Francheteau (1970). These models yield low estimates (22-31 km) for the thickness of the lithosphere. The heat-source distributions of Pollack and Chapman (1977) would yield even lower estimates because more heat flow must come from the base of the lithosphere, and, with fixed conductivity, the lithosphere must be thinner.

Lithosphere-thickness estimates for oceanic crust are generally considerably greater, even near active spreading centers, and are from 35 to 150 km (Froidevaux and others, 1977; Pollack and Chapman, 1977). I would further expect much more extensive volcanism on the shelf and coastal plain if the solidus temperatures were reached at such shallow depths. Petrologic studies of the Quaternary basalts and their harzburgite inclusions (Ghent and others, 1979) suggest that the basalts equilibrated at pressures of 10 to 20 kbar and temperatures of 1,000° to 1,300°C; this regime suggests depths of 30 to 60 km.

A second static model is evaluated that is time-dependent and in which sea-floor spreading is partly accounted for by including as the initial temperature distribution the geotherm that would be expected at Mansiyah I at the end of stage 1 spreading. The temperature distribution of Sclater and Francheteau (1970) is used as the initial condition, and heat-flow and temperature-depth profiles at various times after cessation of spreading are computed. The analytical solution for this model is presented in appendix 1. A spreading rate of 1.96 cm y^{-1} is used, with 1,350°C as the isothermal condition at the base of a lithosphere that is 100 km thick. A constant heat-source distribution of 0.1 HFU is included in the initial condition. Heat-flow and temperature-depth profiles for this model are shown in figure 8, where it can be seen that 10 Ma is the maximum length of time since cessation of spreading for which the observed heat flow within uncertainties can be matched. Because I believe that spreading for stage 1 stopped about 15 Ma ago, it seems that this model will not adequately explain the heat-flow observations.

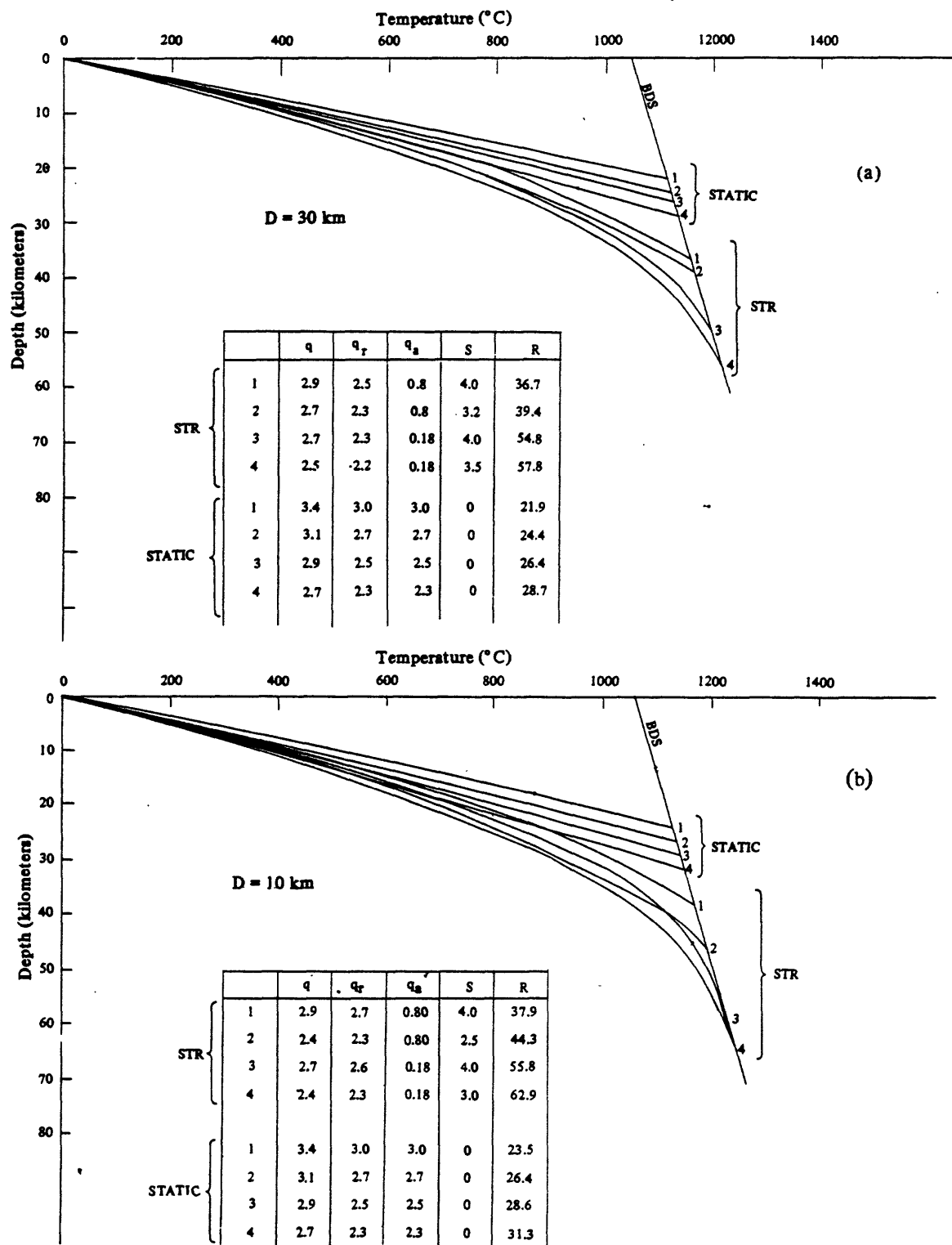


Figure 7.—Graphs showing geotherm estimates for the shelf and coastal-plain areas of oceanic crust for two heat-source distributions. Curves labelled “STATIC” are for a model with no convective flow, whereas those labelled “STR” include solid-state accretion of material at the base of the lithosphere from material flow according to the model of Lachenbruch and Sass (1978). The models are for the most probable set of parameters and for the range of reduced heat flows (2.3-3.1 HFU) thought to be likely for the stage 1 oceanic crust. In both models the thermal conductivity is $6.4\text{E-}3 \text{ cal cm}^{-1}\text{s}^{-1}\text{°C}^{-1}$, density is 3.2 g cm^{-3} and specific heat is 0.27 cal g^{-1} . In 7a, the exponential heat-source distribution parameters are $A_0=1.2 \text{ HGU}$ and $D = 30 \text{ km}$; in 7b, D is reduced to 10 km . “BDS” represents the linear approximation of the dry basalt solidus used to define the base of the lithosphere.

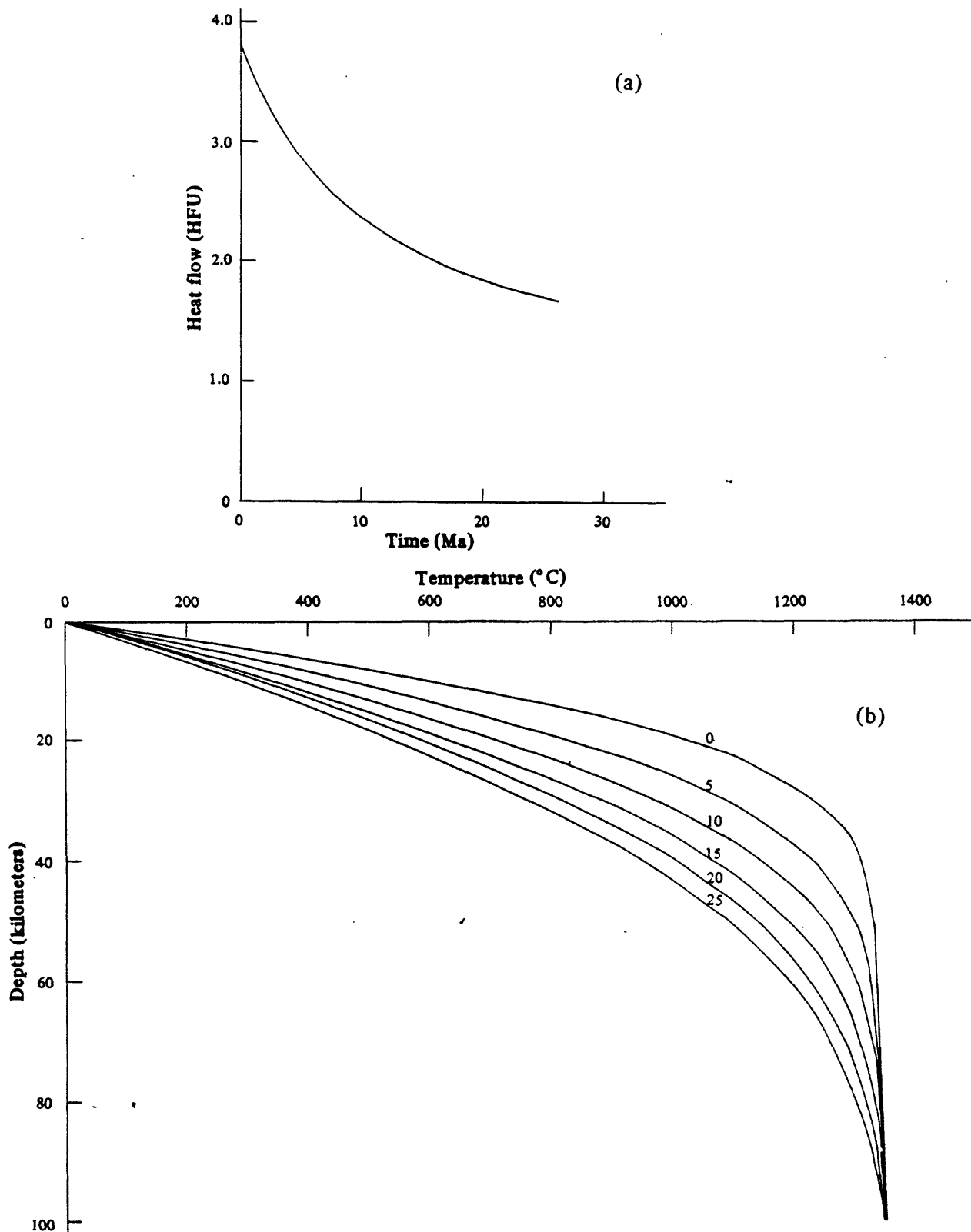


Figure 8.—Plots showing heat-flow (a) and temperature-depth (b) curves at various times for cooling of a horizontal sheet whose surfaces are held at constant temperatures and whose initial temperature distribution is given by the model of Sclater and Francheteau (1970). In (a), the surface heat flow is shown as a function of time, and in (b), the temperature-depth curves for several times are displayed. Numbers on the curves are the time in millions of years since the initial temperature distribution. Parameters for this case (see fig. 10 and appendix 1) are $K=0.006 \text{ cal cm}^{-1} \text{ s}^{-1} \text{ }^{\circ}\text{C}^{-1}$, $\rho=3.3 \text{ g cm}^{-3}$, $c=0.25 \text{ cal g}^{-1}$, $\ell=100 \text{ km}$, $\theta_1=1350^{\circ}\text{C}$, and $\theta_2=0^{\circ}\text{C}$.

Dynamic models for the oceanic crust

I now turn to models that include in some form the effects of convection in the spreading process. For the presently active, deep-water trough, a model is computed using the formulation of Sclater and Francheteau (1970), with a lithosphere that is 100 km thick and that has a temperature of 1,300°C at its base, a conductivity of 0.006 cal cm⁻¹s⁻¹°C⁻¹, a volumetric specific heat of 0.823 cal cm⁻³, a constant heat production of 0.1 HGU, an adiabatic gradient at the spreading axis of 0.3°C km⁻¹, and a velocity of 0.8 cm y⁻¹. For crust 3 to 5 Ma old, the heat flow computed from this model is 5.6 to 4.2 HFU. Variations of parameter values within reasonable limits produce heat flows from about 3.5 to 6.0 HFU for these ages, and for our purposes this model adequately fits the heat flow of stage 2 spreading; however, near the spreading center it fails to represent adequately the observations because it takes no account of hydrothermal circulation.

Next I examine a limiting-case model, in which I ignore the details of two-stage spreading and simply assume that spreading has been continuous for about the last 30 Ma. I assume that spreading began 29 Ma ago (the date of the earliest volcanism of the As Sarat volcanic field) and continuously created a plate of 190 km half-width; these assumptions yield a spreading half-rate of 0.65 cm y⁻¹. All other parameters are as enumerated above. This model yields a heat flow at Mansiyah I of 1.95 HFU, which is substantially less than the 2.65 HFU observed, even considering uncertainties. I thus conclude that either the duration of spreading was much less, for example about 20 Ma, or the model is inappropriate. Inasmuch as a considerable body of geological and geophysical evidence supports the concept of a 30-Ma period of spreading, I prefer the latter alternative. Another possibility for explaining the higher observed heat flow is postspreading intrusive activity in the vicinity of Mansiyah I. However, heat-flow values at other locations on the shelf on the western side of the Red Sea (fig. 2) are for the most part even higher, so such activity would be required to be ubiquitous; furthermore, no surface expression of volcanism is present on the shelf or coastal plain except near Precambrian outcrops. I therefore seek to explain the high heat flow by a more general mechanism, namely, convective flow below the lithosphere. In view of the broad horizontal scale of the system and the large wavelength of regional uplift, I intuitively suspect that mass flow in the upper mantle is still important beneath the shelf areas and possibly beneath the Precambrian shield.

In order to determine if inclusion of flows with reasonable assumed velocities will yield the observed ranges of heat flow, I apply the models of Lachenbruch and Sass (1978). In the case of the shelf areas, I regard the case of solid-state accretion to the base of the lithosphere (the "STR" mode of Lachenbruch and Sass, 1978) as the most plausible model, although I examine modes including intrusive activity as well.

These models once again define the base of the lithosphere as the intersection of the geotherm with the basalt dry solidus; here I use the

same solidus curve as given by equation (5). The models are a function of strain rate, heat flux from the asthenosphere, reduced heat flow, and lithosphere thickness, with thermal conductivity, specific heat, density, heat-source distribution (exponential), and latent heat as parameters. The reduced heat flow and strain rate are reasonably well known, and asthenosphere heat flux and lithosphere thickness are to be determined. The relevant parameters have been estimated above except for latent heat for the intrusive models, which is assumed to be 100 cal g⁻¹, a reasonable value for magmas of basaltic composition.

A parameter-variation study was carried out in which the parameters ranged over the three heat-source distributions named above, and thermal conductivity, density, and specific heat were varied \pm 30 percent. For each case, the asthenosphere flux and strain rate were specified, and the lithosphere thickness and reduced heat flow were determined. Cases were evaluated for asthenosphere flux varying from 0.1 to 1.0 HFU and strain rate varying from 0.5 to 5.0 percent per Ma. In principle, this process should determine asthenosphere flux and lithosphere thickness because reduced heat flow and strain rate are known. In practice, however, asthenosphere flux is not a strong function of reduced heat flow for a given strain rate, and the uncertainties in reduced heat flow and strain rate obviate any better determination of asthenosphere flux than that inherent in the model, that is, a minimum value of 0.18 HFU due to the solidus gradient and a possible maximum of about 0.8 to 1.0 HFU, the values of the nearby Shield. The results of these models place limits of about 30 to 64 km on the thickness of the lithosphere, with values near 30 km being obtained when the strain rate, asthenosphere flux, and reduced heat flow are all at their highest values. For the models that include intrusive activity, the reduced heat flow is substantially increased and lithosphere thicknesses decreased for a given strain rate and asthenosphere flux.

Ranges of geotherms for two heat-source distributions and the thermal-conductivity, density, and specific-heat values estimated above are shown in figures 7a and 7b. Inspection of these curves and the values of the variables shows that values of the strain rate must be 3 percent per Ma or greater unless the asthenosphere flux is 0.8 HFU or greater. It is also apparent that it probably is not possible to obtain the upper limiting values of the Red Sea shelf heat flow (3.0 HFU or greater) within the constraints of the parameter and variable ranges considered. Strain rates in excess of 4 percent per Ma are probably too high; thus, asthenosphere flux and the radiogenic heat-source distribution are the only obvious ways to increase the heat flow. Considering the distributions used here and the thick sedimentary blanket on the shelf, the radiogenic contributions to the heat flow I have calculated probably represent minimum contributions. Alternatively, the upper bound on asthenosphere heat flux in the oceanic crust is by no means understood, and perhaps an even greater contribution than the 0.8 HFU value assumed here is appropriate.

In any event, I have shown that by accounting for the observed plate motion by mass flow, I can account for the observed heat-flow values on the Red Sea shelf and coastal plain using values of physical properties

that are reasonable within my current ability to estimate them. Further, dynamic models seem to be required because efforts to match the heat flow at Mansiyah I with static models have not proved successful and, according to presently available data, Mansiyah I probably represents a minimum average surface heat flow for the stage 1 lithosphere.

Edge effects at shot point 5

The heat-flow observation at shot point 5 is the only one in the Shield that can be regarded as anomalous within the uncertainties of these measurements. Because the nearby oceanic plate (10 km distant) is known to be an area of high heat flow, I seek to explain the heat flow at shot point 5 in terms of heating by the emplacement of the oceanic crust.

A suitable model for this situation might be a homogeneous quarter-space (that is, a two-dimensional region extending to infinity from the origin in the +x and +z directions; see fig. 11), whose surface temperature (z=0) is zero and whose initial temperature distribution is a linear function of depth. This model initially has a constant heat flow, which I will set equal to a characteristic value for the Shield, for example, 0.8 or 1.0 HFU. At the vertical boundary of the quarter-space (x=0), I impose as a boundary condition a temperature that is a second linear function of depth; then as a function of time I can observe the heating or cooling of the quarter-space depending on whether the boundary temperature gradient is greater or less than the initial one. The solution to this problem may be available in the literature, but I have been unable to locate it. However, the solution is straightforward and is presented in appendix 2. I obtain for the heat flow on the surface (z=0):

$$q(x,0,t; A,B,K, \rho, c) = KA + K(B-A) \operatorname{erf} \frac{x}{2(kt)^{1/2}} \quad (6)$$

where $k=K/(\rho c)$ and A and B are the boundary and initial thermal gradients, respectively.

A parameter-variation study was done for this model, using values for A of 30, 40, and 50°C km⁻¹, values for K of 0.005 and 0.009 cal cm⁻¹s⁻¹°C⁻¹, and values for B such that KB is 0.8, 1.0, and 1.2 HFU. Values of ρ and c appropriate for shield-type rocks, 2.73 g cm⁻³ and 0.27 cal g⁻¹, were used for all models. A representative set of these calculations for several time intervals is shown in figure 9. It is immediately obvious that the shapes of the curves are diagnostic of the time since heating began. If such a simple model were to pertain approximately to the boundary-zone area, then a detailed (5-10 km spacing) heat-flow profile perpendicular to the boundary might provide important evidence on the times of emplacement of the oceanic crust.

In figure 9, shot point 5 probably falls in the 5- to 20-km-distance coordinate interval. Tertiary dikes are present only 5 km southwest of shot point 5; however, the actual oceanic crust

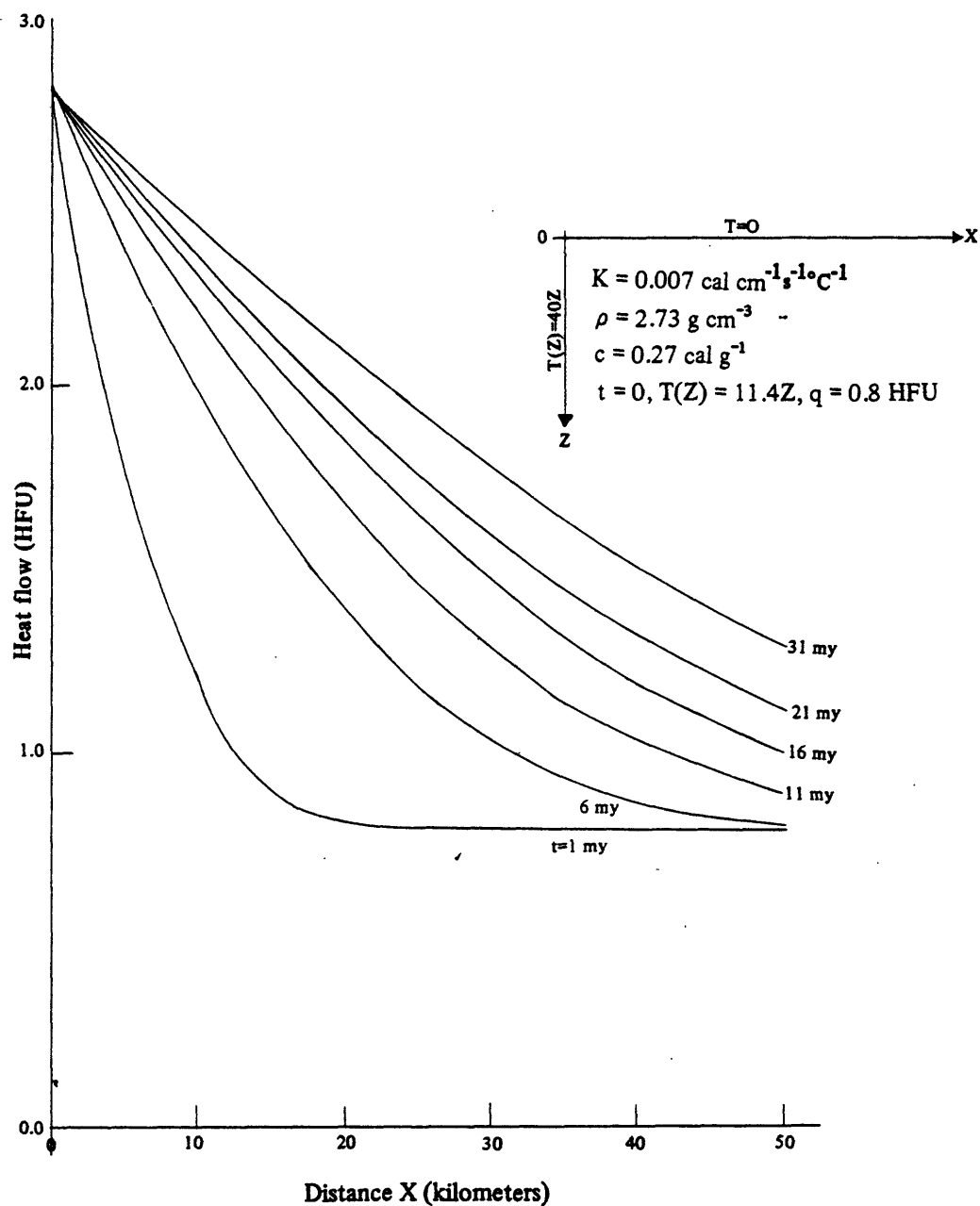


Figure 9.—Plots of surface heat flow as a function of distance from the $x = 0$ boundary for several times for the heating of a homogeneous quarter-space. Numbers on each curve are the time in millions of years since initiation of heating. The position of shot point 5 relative to the oceanic plate is in the 5-20 km interval of the distance axis (see text).

may be as far away as 20 km. The situation is further complicated by the fact that this area is a "corner" of left-lateral offset of the oceanic crust; in fact, this area is the southern limit of a proposed transform fault zone (Hall, 1980). Thus the two-dimensional model is not strictly applicable here and represents an upper limit to heat flow from heating. Nonetheless, from the figure, this case corresponds reasonably well with my model of initial emplacement about 30 Ma ago. By small variations of the parameters, one can adjust the heat flow at a given time within fairly broad limits (± 0.4 HFU). Thus one can fit the heat flow at shot point 5 after 10 to 30 Ma using reasonable parameter values. However, quite radical parameter changes are required to fit the shot point heat-flow values after only 5 Ma.

SUMMARY

Present geological and geophysical evidence depicts the Red Sea-Arabian Peninsula system as one which has undergone several periods of active sea-floor spreading during the last 30 Ma. I interpret this system to be the surface manifestation of a large-scale mantle-flow process in which mantle is flowing upward in the area of the Red Sea, gradually becoming horizontal as one progresses eastward, and then, as indicated by uplift and deformation rates in the Zagros Mountains of Iran (Falcon, 1974; Vita-Finzi, 1979), becoming downward in that region. Such a model explains the broad regional uplift observed, as well as the sea-floor spreading phenomena.

Combined seismic refraction, gravity, and surface geologic studies have resulted in a preliminary crustal section that is not likely to be grossly in error. Within this framework I have demonstrated that the available heat-flow data, within their uncertainties, are compatible with this model.

Heat flow-heat production data for sites in plutonic rocks on the Arabian Shield (~ 1 HFU, 2-4 HGU) give reasonable geotherm estimates; the geotherms at shot points 2 and 3 are virtually identical within uncertainties, but the geotherm at shot point 4 is significantly hotter. Average heat-flow values (4 HFU) in the deep-water, actively spreading trough area can be adequately explained by moving-slab models such as that of Sclater and Francheteau (1970).

Heat-flow models of the older oceanic crust evidently require some form of convective heat transfer at the base of the lithosphere to account for the high heat flows observed on the shelf and coastal plain (2.7-3.0 HFU). The solid-state accretion model of Lachenbruch and Sass (1978) seems to adequately fit the data, and lithosphere-thickness estimates for the most probable parameter sets range from 37 to 63 km. Heat flux into the base of the lithosphere is essentially unconstrained, but the models indicate that a value of 0.8 HFU or more is required.

Finally, conductive heating of the edge of the Precambrian crust by the abutting oceanic crust 10 to 30 Ma after emplacement of oceanic crust, together with a heat-flow component characteristic of the Shield, is adequate to explain the heat flow (2.0 HFU) observed at shot point 5.

REFERENCES CITED

- Anderson, R. E., 1979, Geology of the Wadi 'Atf (sheet 17/43 A) and Mayza' (sheet 17/43 B) quadrangles, Kingdom of Saudi Arabia: Saudi Arabian Directorate General of Mineral Resources Bulletin 25, 33 p.
- Bartholomew (John) and Son, Ltd., 1977, The Times Atlas of the World: New York, Quadrangle-The New York Times Book Company, 223 p.
- Benfield, A. E., 1949, The effect of uplift and denudation on underground temperatures: Journal of Applied Physics, v. 20, p. 66-70.
- Birch, F., 1948, The effects of Pleistocene climatic variations upon geothermal gradients: American Journal of Science, v. 246, p. 729-760.
- Blank, H. R., Jr., Anderson, R. E., Andreasen, G. E., Gettings, M. E., Girdler, R. W., Greenwood, W. R., Hadley, D. G., Hall, S. A., and Schmidt, D. L., 1975, First-stage spreading of the Red Sea: a new analysis [abs.]: International Union of Geodesists and Geophysicists meeting, Grenoble, France, 1975, Abstracts volume.
- Blank, H. R., Jr., Gettings, M. E., and Andreasen, G. E., 1979a, Tertiary continental margin in southwest Saudi Arabia; status of current investigations: EOS, Transactions of American Geophysical Union, v. 60, p. 375.
- Blank, H. R., Healy, J. H., Roller, John, Lamson, Ralph, Fisher, Fred, McClearn, Robert, and Allen, Steve, 1979b, Seismic refraction profile, Kingdom of Saudi Arabia--field operations, instrumentation, and initial results: U.S. Geological Survey Open-File Report 79-1568, 49 p.
- Brown, G. F., 1972, Tectonic map of the Arabian Peninsula: Saudi Arabian Directorate General of Mineral Resources Arabian Peninsula map AP-2, scale 1:4,000,000.
- Carslaw, H. S., and Jaeger, J. C., 1959, Conduction of heat in solids: Oxford, Clarendon Press, 510 p.
- Clark, S. P., Jr., 1966, Thermal conductivity, section 21, in Handbook of physical constants: Geological Society of America Memoir 97, p. 459-482.
- Coleman, R. G., Fleck, R. J., Hedge, C. E., and Ghent, E. D., 1977, The volcanic rocks of southwest Saudi Arabia and the opening of the Red Sea, in Red Sea Research 1970-1975: Saudi Arabian Directorate General of Mineral Resources Bulletin 22, p. D1-D30.
- Coleman, R. G., Hadley, D. G., Fleck, R. G., Hedge, C. T., and Donato, M. M., 1979, The Miocene Tihama Asir ophiolite and its bearing on the opening of the Red Sea, in Evolution and mineralization of the Arabian-Nubian Shield: King Abdulaziz University, Institute of Applied Geology Bulletin 3, v. 1: Oxford-New York, Pergamon Press, p. 173-185.

- Davis, E. E., and Lister, C. R. B., 1974, Fundamentals of ridge crest topography: *Earth and Planetary Science Letters*, v. 21, p. 405-413.
- Falcon, N. L., 1974, Southern Iran, Zagros mountains, in Spencer, A. M., ed., *Mesozoic-Cenozoic orogenic belts: Geological Society of London Special Publication no. 4*, p. 199-211.
- Froidevaux, C., Schubert, G., and Yuen, D. A., 1977, Thermal and mechanical structure of the upper mantle; a comparison between continental and oceanic models: *Tectonophysics*, v. 37, p. 233-246.
- Gettings, M. E., 1977, Delineation of the continental margin in the southern Red Sea region from new gravity evidence, in *Red Sea Research 1970-1975: Saudi Arabian Directorate General of Mineral Resources Bulletin 22*, p. K1 - K11.
- Gettings, M. E., and Showail, Abdullah, 1982, Heat-flow measurements at shot points along the 1978 Saudi Arabian seismic deep-refraction line, part 1: Results of the measurements: U.S. Geological Survey Open-File Report 82-793, 108 p.
- Ghent, E. C., Coleman, R. G., and Hadley, D. G., 1979, Ultramafic inclusions and host alkali olivine basalts of the southern coastal plain of the Red Sea, Kingdom of Saudi Arabia: U.S. Geological Survey Saudi Arabian Project Report 244, 37 p.
- Gillman, M., 1968, Primary results of a geological and geophysical reconnaissance of the Jizan coastal plain in Saudi Arabia: American Institute of Mining and Metallurgical Engineers, Society of Petroleum Geologists, Saudi Arabian Section, 2nd Regional Symposium, Dhahran, Proceedings, p. 189-208.
- Girdler, R. W., 1970, A review of Red Sea heat flow: *Philosophical Transactions of the Royal Society of London*, v. 267, p. 191-203.
- Girdler, R. W., Brown, C., Noy, D. J. M., and Styles, P., 1980, A geophysical survey of the westernmost Gulf of Aden: *Philosophical Transactions of the Royal Society of London*, v. 298, p. 1-43.
- Girdler, R. W., and Evans, T. R., 1977, Red Sea heat flow: *Geophysical Journal of the Royal Astronomical Society*, v. 51, p. 245-251.
- Girdler, R. W., and Styles, P., 1974, Two stage Red Sea floor spreading: *Nature*, v. 247, p. 7-11.
- Greenwood, W. R., and Anderson, R. E., 1977, Palinspastic map of the Red Sea prior to Miocene sea floor spreading, in *Red Sea Research 1970-1975: Saudi Arabian Directorate General of Mineral Resources Bulletin 22*, p. Q1-Q5.
- Hadley, D. G., 1975, Geology of the Wadi Hali quadrangle, sheet 18/41 B, Kingdom of Saudi Arabia, with a section on Aeromagnetic investigations, by G. E. Andreason: Saudi Arabian Directorate General of Mineral Resources Geologic Map GM-21, 19 p., scale 1:100,000.

- _____, 1980, Reconnaissance geology of the Musaylim quadrangle, sheet 19/40 B, Kingdom of Saudi Arabia: Saudi Arabian Directorate General of Mineral Resources Geologic Map GM-34, 7 p., scale 1:100,000.
- Hadley, D. G., and Fleck, R. J., 1980a, Reconnaissance geology of the Al Lith quadrangle, sheet 20/40 C, Kingdom of Saudi Arabia: Saudi Arabian Directorate General of Mineral Resources Geologic Map GM-32, 10 p., scale 1:100,000.
- _____, 1980b, Reconnaissance geology of the Jabal 'Afaf quadrangle, sheet 20/40 D, Kingdom of Saudi Arabia: Saudi Arabian Directorate General of Mineral Resources Geologic Map GM-33, 10 p., scale 1:100,000.
- Hall, S. A., 1980, A total intensity magnetic anomaly map of the Red Sea and its interpretation: U.S. Geological Survey Open-File Report 80-131, 260 p.
- Hall, S. A., Andreasen, G. E., and Girdler, R. W., 1977, Total-intensity magnetic anomaly map of the Red Sea and adjacent coastal areas, a description and preliminary interpretation, in Red Sea research 1970-1975: Saudi Arabian Directorate General of Mineral Resources Bulletin 22, p. F1-F15.
- Hotzl, H., and Zotl, J. G., 1978, Climatic changes during the Quaternary period, in Al-Sayari, S. S., and Zotl, J. G., eds., Quaternary period in Saudi Arabia: New York, Springer-Verlag, p. 301-311.
- Jaeger, J. C., 1965, Application of the theory of heat conduction to geothermal measurements, chapter 2, in Lee, W. H. K., ed., Terrestrial heat flow: American Geophysical Union, Geophysical Monograph 8, p. 7-23.
- Kelley, K. K., 1960, Contributions to the data on theoretical metallurgy; 13--High temperature heat-content, heat-capacity, and entropy data for the elements and inorganic compounds: U.S. Bureau of Mines Bulletin 584, 232 p.
- Lachenbruch, A. H., 1970, Crustal temperature and heat production; implications of the linear heat flow relation: Journal of Geophysical Research, v. 75, p. 3291-3300.
- Lachenbruch, A. H., and Sass, J. H., 1977, Heat flow in the United States and the thermal regime of the crust, in Heacock, J. G., ed., The Earth's crust: American Geophysical Union, Geophysical Monograph 20, p. 626-675.
- _____, 1978, Models of an extending lithosphere and heat flow in the basin and range province, in Smith, R. B., and Eaton, G. P., eds., Cenozoic tectonics and regional geophysics of the western Cordillera: Geological Society of America Memoir 152, p. 209-250.

- Le Pichon, Xavier, Francheteau, Jean, and Bonnin, Jean, 1976, Plate tectonics (2nd ed.): Amsterdam, Elsevier, 311 p.
- Madden, C. T., Naqvi, I. M., Whitmore, F. C., Schmidt, D. L., Langston, Wann, Jr., and Wood, R. C., 1980, Paleocene vertebrates from coastal deposits in the Harrat Haddan area, At Taif region, Kingdom of Saudi Arabia: U.S. Geological Survey Open-File Report 80-227, 29 p.
- McKenzie, D. P., 1967, Some remarks on heat flow and gravity anomalies: Journal of Geophysical Research, v. 72, p. 6261-6273.
- Murase, Tsutomu, and McBirney, A. R., 1973, Properties of some common igneous rocks and their melts at high temperatures: Geological Society of America Bulletin, v. 84, p. 3563-3592.
- Nafe, J. E., and Drake, C. L., 1968, Physical properties of rocks of basaltic composition, in Hess, H. H., and Polderwaart, A., eds., Basalts: The Polderwaart treatise on rocks of basaltic composition, v. 2: New York, Interscience Publishers, p. 483-502.
- Overstreet, W. C., Stoesser, D. B., Overstreet, E. F., and Goudarzi, G. H., 1977, Tertiary laterite of the As Sarat Mountains, Asir Province, Kingdom of Saudi Arabia: Saudi Arabian Directorate General of Mineral Resources Bulletin 21, 30 p.
- Parsons, B., and Sclater, J. G., 1977, An analysis of the variation of ocean floor bathymetry and heat flow with age: Journal of Geophysical Research, v. 82, p. 803-827.
- Pollack, H. N., and Chapman, D. S., 1977, On the regional variation of heat flow, geotherms, and lithospheric thickness: Tectonophysics, v. 38, p. 279-296.
- Powers, R. W., Ramirez, L. F., Redmond, C. D., and Elberg, E. L., Jr., 1966, Geology of the Arabian Peninsula--sedimentary geology of Saudi Arabia: U.S. Geological Survey Professional Paper 560-D, 147 p.
- Schmidt, D. L., Hadley, D. G., and Stoesser, D. B., 1978, Late Proterozoic crustal history of the Arabian Shield, southern Najd province, Kingdom of Saudi Arabia, in Evolution and mineralization of the Arabian-Nubian Shield, v. 2: Oxford-New York, Pergamon Press, p. 41-58.
- Sclater, J. G., and Francheteau, J., 1970, The implications of terrestrial heat flow observations on current tectonic and geochemical models of the crust and upper mantle of the earth: Geophysical Journal of the Royal Astronomical Society, v. 20, p. 509-542.
- Skinner, B. J., 1966, Thermal expansion, section 6, in Clark, S. P., ed., Handbook of physical constants: Geological Society of America Memoir 97, p. 78-96.

- Smith, D. L., Nuckels, C. E., III, Jones, R. L., and Cook, G. A., 1979, Distribution of heat flow and radioactive heat generation in northern Mexico: *Journal of Geophysical Research*, v. 84, p. 2371-2379.
- Smith, J. W., 1980, reconnaissance geologic map of the Wadi Mahani quadrangle, sheet 22/40 A, Kingdom of Saudi Arabia: Saudi Arabian Directorate General of Mineral Resources Geologic Map GM-35, 18 p., scale-1:100,000.
- U.S. Geological Survey, 1972, Topographic map of the Arabian Peninsula: Saudi Arabian Directorate General of Mineral Resources Arabian Peninsula Map AP-1, scale 1:4,000,000.
- Vita-Finzi, C., 1979, Rates of Holocene folding in the coastal Zagros near Bandar-Abbas, Iran: *Nature*, v. 278, p. 632-634.
- Worzel, J. L., 1974, Standard oceanic and continental structure, in Burke, C. A., and Drake, C. L., eds., *Geology of continental margins*: New York, Springer-Verlag, p. 59-66.

Appendix 1.--Static cooling of an infinite sheet with isothermal surfaces and an initial temperature distribution given by the model of Sclater and Francheteau (1970)

We seek to solve the transient heat-flow equation

$$\frac{\partial \Theta}{\partial t}(x, t) = k \frac{\partial^2 \Theta}{\partial x^2}(x, t) \quad (0 < x < l) \quad (7)$$

for the geometry shown in figure 10. The parameter k is the thermal diffusivity, $k = K/\rho c$. The boundary conditions for this problem are

$$\Theta(0, t) = \Theta_1 \text{ and } \Theta(l, t) = \Theta_2 \quad (8)$$

and the initial condition (Sclater and Francheteau, 1970) is

$$\begin{aligned} \Theta(x', 0) = \Theta_1 + \frac{C_{-1}(\Theta_1 - \Theta_2)}{l^2} x'^2 - \frac{C_0(\Theta_1 - \Theta_2)}{l} x' \\ + \sum_{n=1}^{\infty} C_n \sin \frac{n\pi x'}{l} \equiv f(x') \end{aligned} \quad (9)$$

where

$$\begin{aligned} C_{-1} &= \frac{-Hl^2}{2K(\Theta_1 - \Theta_2)} \\ C_0 &= 1 + C_{-1} \end{aligned} \quad (10)$$

and

$$\begin{aligned} C_n = \left[\frac{2(-1)^{n+1}}{n\pi} \left(1 - \frac{l\alpha}{\Theta_1 - \Theta_2} \right) + \frac{4C_{-1}}{n^3\pi^3} (1 - (-1)^n) \right] (\Theta_1 - \Theta_2) \\ \exp \left[\frac{R - (R^2 + n^2\pi^2)^{1/2}S}{l} \right] \end{aligned} \quad (11)$$

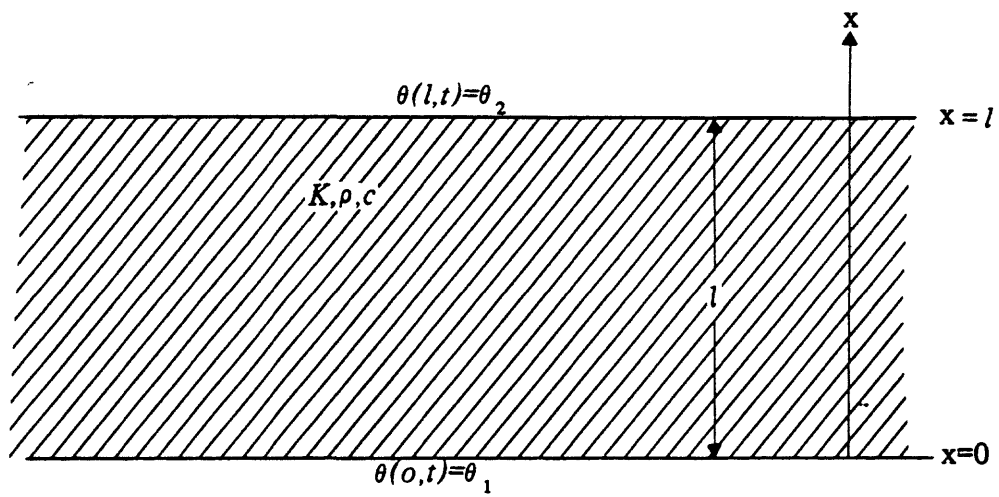


Figure 10.—Geometric relationships and parameters for the static cooling of a horizontal sheet.

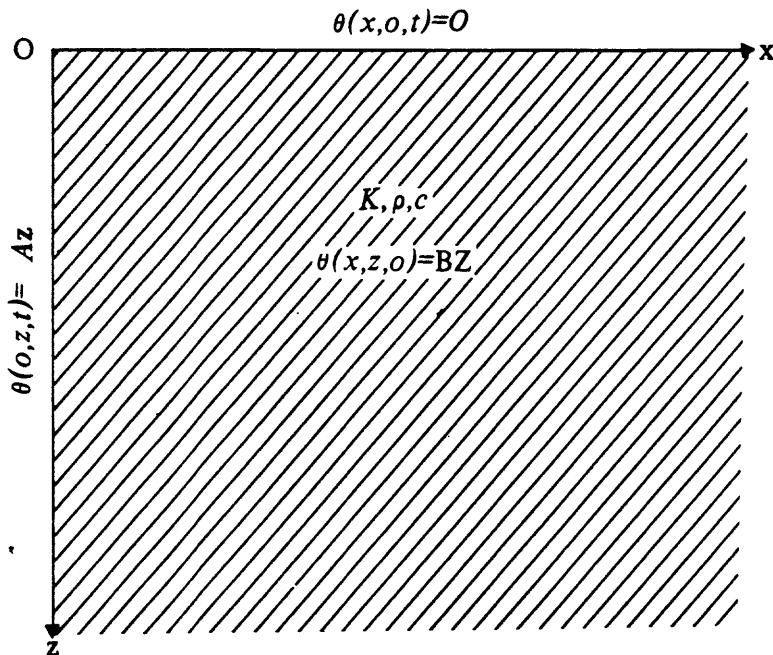


Figure 11.—Geometric relationships and parameters for a homogeneous quarter-space.

In these equations, α is the adiabatic temperature gradient, K the thermal conductivity, S is the distance from the ridge axis (spreading center) and R is the thermal Reynolds number

$$R = \frac{v\ell}{2k}, \quad (12)$$

where v is the spreading velocity (half-rate). H is the radiogenic heat production. Note that these parameters for equations (9) to (12) merely establish the initial temperature distribution and that heat production is not included in the model.

Following Carslaw and Jaeger (1959, section 3.4) the general Fourier series solution to this system is given by

$$\begin{aligned} \Theta(x,t) = & \Theta_1 + (\Theta_2 - \Theta_1) \frac{x}{\ell} + \frac{2}{\pi} \sum_{n=1}^{\infty} \frac{(-1)^n \Theta_2 - \Theta_1}{n} \exp \left(\frac{-kn^2 \pi^2 t}{\ell^2} \right) \\ & \sin \left(\frac{n\pi x}{\ell} \right) + \frac{2}{\ell} \sum_{n=1}^{\infty} \exp \left(\frac{-kn^2 \pi^2 t}{\ell^2} \right) \sin \left(\frac{n\pi x}{\ell} \right) \int_0^{\ell} f(x') \sin \left(\frac{n\pi x'}{\ell} \right) dx'. \quad (13) \end{aligned}$$

Substituting equation (12) into (13) and effecting the integration yields for the temperature

$$\begin{aligned} \Theta(x,t) = & \Theta_1 - (\Theta_1 - \Theta_2) \frac{x}{\ell} + \frac{2}{\pi} (\Theta_1 - \Theta_2) \sum_{n=1}^{\infty} \frac{1}{n} \frac{-2C_{-1} (1 - (-1)^n)}{n^2 \pi^2} \\ & + \left\{ \left(1 - \frac{\ell \alpha}{\Theta_1 - \Theta_2} \right) (-1)^{n+1} + \frac{2C_{-1}}{n^2 \pi^2} (1 - (-1)^n) \right\} \exp \left[\frac{R - (R^2 + n^2 \pi^2)^{1/2} S}{\ell} \right] \\ & \sin \left(\frac{n x}{\ell} \right) \exp \left(-\frac{kn^2 \pi^2 t}{\ell^2} \right). \quad (14) \end{aligned}$$

Differentiation and substitution of $x = \ell$ yields for the heat flow at the upper surface

$$\begin{aligned}
 q(\ell, t) = & -K \left[-\frac{(\Theta_1 - \Theta_2)}{\ell} + \frac{2}{\ell} (\Theta_1 - \Theta_2) \sum_{n=1}^{\infty} \frac{2C_{-1} (1 - (-1)^n)}{n^2 \pi^2} \right. \\
 & \left. - \left\{ \left(1 - \frac{\ell \alpha}{\Theta_1 - \Theta_2} \right) + \frac{2C_{-1}}{n^2 \pi^2} (1 - (-1)^n) \right\} \exp \left(\frac{R - (R^2 + n^2 \pi^2)^{1/2}}{\ell} S \right) \right. \\
 & \left. \exp \left(-\frac{kn^2 \pi^2 t}{\ell^2} \right) \right] . \quad (15)
 \end{aligned}$$

Equations (14) and (15) can be evaluated to any desired degree of accuracy by evaluating the appropriate number of terms in the Fourier series. For the parameter values used in this report, typically 8 or 9 terms are required in equation (14) to attain a change in successive terms of less than $5E-4$.

Appendix 2.--Temperature and heat flow of a homogeneous quarter-space

We seek to solve

$$k \nabla^2 \Theta(x, z, t) = \frac{\partial \Theta(x, z, t)}{\partial t}, \quad x, z, t > 0 \quad (16)$$

for the geometry shown in figure 11. We do not include a heat-source term as we expect to apply this model only to the upper few kilometers of the Earth's crust, and such a heat flow can be included in the boundary condition. The boundary conditions are

$$\Theta(0, z, t) = A z, \quad (17)$$

$$\Theta(x, 0, t) = 0, \quad (18)$$

and $\Theta(x \rightarrow \infty, z, t) = B z. \quad (19)$

The initial condition is

$$\Theta(x, z, 0) = B z. \quad (20)$$

As before, $k = K/\rho c$, the thermal diffusivity.

The procedure of Carslaw and Jaeger (1959, section 1.14.1) may be applied to split the solution into two functions, one a steady-state solution of Poisson's equation satisfying the boundary conditions and one a transient solution of the heat-conduction equation satisfying a function of the initial conditions with zero boundary conditions. Thus we let

$$\Theta(x, z, t) = u(x, z) + w(x, z, t) \quad (21)$$

where u satisfies

$$\nabla^2 u = 0 \quad (22)$$

throughout the solid and equations (17) to (19) at the boundaries.

We also require w to satisfy

$$k \nabla^2 w - \frac{\partial w}{\partial t} = 0 \quad (23)$$

with $w = 0$ at the boundaries and initial condition

$$w = Bz - u. \quad (24)$$

Assuming $u(x, z)$ to be a product function

$$u(x, z) = \psi(x) \phi(z) \quad (25)$$

leads to

$$u(x, z) = \left(\frac{B-A}{L} x + A \right) z \quad (26)$$

where L is an arbitrarily large value of x ; thus the initial condition on w is

$$w(x, z, 0) = Bz - z \left(\frac{B-A}{L} x + A \right) = z \left\{ B-A - \frac{B-A}{L} x \right\}. \quad (27)$$

This is a product function of x and z , and thus a solution for w may be sought by separation of variables

$$w(x, z, t) = \psi'(x, t) \phi'(z, t)$$

where the functions ψ' and ϕ' are both solutions of

$$k \frac{\partial^2 \chi}{\partial y^2} - \frac{\partial \chi}{\partial t} = 0 \quad (28)$$

and where the spatial variable y is x when χ is ψ' , and y is z when χ is ϕ' .

The general solution for this case is (Carslaw and Jaeger, 1959, section 2.4)

$$\psi'(x, t) = \frac{1}{2(\pi kt)^{1/2}} \int_0^\infty f(x') \left\{ \exp \frac{-(x-x')^2}{4kt} - \exp \frac{-(x+x')^2}{4kt} \right\} dx'. \quad (29)$$

In this case (for Ψ'),

$$f(x') = (B-A) - \left(\frac{B-A}{L}\right) x'; \quad (30)$$

and for the case of Φ' ,

$$f(z') = z'. \quad (31)$$

After effecting the necessary integrations and with some algebra, we finally obtain for the temperature distribution

$$\Theta(x,z,t) = Az + (B-A)z \operatorname{erf} \frac{x}{2(kt)^{1/2}} \quad (32)$$

where the erf is the error function

$$\operatorname{erf}(u) = \frac{2}{\sqrt{\pi}} \int_0^u e^{-\xi^2} d\xi. \quad (33)$$

Partial differentiation of (32) with respect to z yields the surface heat flow given in equation (6).